Response to all referees and explanation of the revision.

Dear Editor,

We thank the referees and others who helped to improve the manuscript, the revision includes all the suggestions and more. All referees had positive comments on the importance of the study and suggested relatively minor revisions and clarifications. Detailed replies to all the comments of the 3 anonymous referees (RC1, RC2, RC4) and two named referees (RC3, SC1) were posted online; we appreciate the great interest the study received from the referees and others (close to 400 views). We also received informal comments (not posted online) from another leading sea level expert, who suggested additional calculations to confirm our results, so additional statistical calculations are added as Supplementary material. The changes in the revised manuscript are detailed in the online replies and highlighted in the "changes" file below.

<u>The main changes in the revised manuscript include:</u>

1. New Fig. 1 that compares the mean SSH of RecSL with AVISO and shows the locations of data and subregions.

2. Additional calculations were performed, first, to compare the EMD correlations with more traditional wavelet coherence calculations, and second, to test the statistics of the reconstructed GS proxy: 1000 simulations with red noise showed that the found "unprecedented" GS weakening is very unlikely to occur by chance. These calculations are added in 3 new Supplementary figures (S1-S3).

3. The structure of the entire manuscript was reorganized, so that validation/evaluation of the reconstruction against data comes first (new section 3.2) and precedes the discussion of mechanisms and basin-scale modes (new section (3.3). The order of sections and all figures was changed accordingly.

4. There are 12 additional references: Bingham and Hughes (2009), Chambers (2015), Dangendorf et al. (2017), Ducet et al. (2000), Grinsted et al. (2004), Holgate et al. (2013), Joyce et al. (2000), Montgomery (1938), Sevellec and Federov (2013), Smeed et al. (2018), Taylor and Stephens (1998), Thiebaux Zwiers (1984).

Global sea level reconstruction for 1900-2015 reveals regional variability in ocean dynamics and an unprecedented long weakening in the Gulf Stream flow since the 1990s

Tal Ezer[1], Sönke Dangendorf[1]

[1]Center for Coastal Physical Oceanography, Old Dominion University
4111 Monarch Way, Norfolk, Virginia, 23508, USA

Corresponding author: Tal Ezer (tezer@odu.edu)

Submitted to *Ocean Science* on March 23, 2020
Reply to reviewers' comments posted June 1 to June 20, 2020
Revision date: June 25, 2020

Abstract. A new monthly global sea level reconstruction for 1900-2015 was analyzed and compared with various observations to examine regional variability and trends in the ocean dynamics of the western North Atlantic Ocean and the U.S. East Coast. Proxies of the Gulf Stream (GS) strength in the Mid-Atlantic Bight (GS-MAB) and in the South Atlantic Bight (GS-SAB) were derived from sea level differences across the GS. While decadal oscillations dominate the 116-year record, the analysis showed an unprecedented long period of weakening in the GS flow since the late 1990s. The only other period of long weakening in the record was during the 1960s-1970s and red noise experiments showed that is very unlikely that those just occurred by chance. Ensemble Empirical Mode Decomposition (EEMD) was used to separate oscillations at different time scales, showing that the low-frequency variability of the GS is connected to the Atlantic Multidecadal Oscillations (AMO) and the Atlantic Meridional Overturning Circulation (AMOC). The recent weakening of the reconstructed GS-MAB was mostly influenced by weakening of the upper mid-ocean transport component of AMOC as observed by the RAPID measurements for 2005-2015. Comparison between the reconstructed sea level near the coast and tide gauge data for 1927-2015 showed that the reconstruction underestimated observed coastal sea level variability for time scales less than ~5 years, but lower frequency variability of coastal sea level was captured very well in both amplitude and phase by the reconstruction. Comparison between the GS-SAB proxy and the observed Florida Current transport for 1982-2015 also showed significant correlations for oscillations with periods longer than ~5 years. The study demonstrated that despite the coarse horizontal resolution of the global reconstruction (1°×1°), long-term variations in regional dynamics can be captured quite well, thus making the data useful for studies of long-term variability in other regions as well.

1. Introduction

Various analyses of tide gauge data show acceleration of global sea level rise over the past century with particularly high rates of rise over the most recent years (Church and White, 2006, 2011; Merrifield et al., 2009; Jevrejeva et al., 2008; Woodworth et al., 2011; Hay et al., 2015; Dangendorf et al., 2017, 2019). However, the presence of pronounced natural variability at various timescales makes the detection of the long-term acceleration due to anthropogenic climate change more difficult with existing sea level data (Kopp, 2013; Dangendorf et al., 2014; Haigh et al., 2014; Kenigson and Han, 2014). Evaluating global sea level acceleration is important for understanding the global climate system but

knowing the mean global sea level rise is insufficient for preparation of coastal communities under threat of increased flooding. Other factors such as land subsidence and ocean and atmospheric dynamics can have significant impact on regional relative sea level rise, introducing substantial differences to global sea level rise (Cazenave and Cozannet, 2014).

The U.S. East Coast is a region that has been recently labeled as a "hotspot for accelerated sea level rise" (Boon, 2012; Ezer and Corlett, 2012; Sallenger et al., 2012; Kopp, 2013; Ezer, 2013; Ezer et al., 2013; Gehrels et al., 2020). Land subsidence associated with the Glacial Isostatic Adjustment (GIA) plus local geological, cryospheric and hydrological processes increase local sea level rise along the U.S. East Coast relative to the global rates (Boon et al., 2010; Kopp, 2013; Miller et al., 2013; Frederikse et al., 2017; Gehrels et al., 2020). An additional factor, less understood, is acceleration/deceleration due to the dynamic response to changes in ocean circulation, for example, a potential slowdown in the GS and AMOC (which the GS is part of) can increase coastal sea level along the western North Atlantic coasts (Ezer and Corlett, 2012; Sallenger et al., 2012; Ezer et al., 2013; Ezer and Atkinson, 2014; Rahmstorf et al., 2015; Little et al., 2019). Therefore, it is important to study regional climatic changes for flood-prone coastal communities. The idea of connections between weakening in the GS strength and rising coastal sea level is not new (Montgomery, 1938; Blaha, 1984) and has been identified in data and ocean models (Ezer, 1999, 2001, 2013, 2015; Ezer at al., 2013; Levermann et al., 2005; Yin et al., 2009; Yin and Goddard, 2013; Goddard et al., 2015). Because sea level is lower/higher on the onshore/offshore side of the GS (by ~1-1.5 m; due to the geostrophic balance), changes in the path and strength of the GS offshore can impact coastal sea level variations along the U.S. East Coast (e.g., see Fig. 2 in Ezer et al., 2013). This connection involves various temporal and spatial scales and complex mechanisms, so detecting the exact connections between changes in the AMOC and the GS and coastal variability is still an ongoing research (e.g., Little et al., 2019; Piecuch et al., 2019). The processes that transfer large-scale open-ocean signals into coherent regional coastal sea level response involve fast-moving barotropic ocean waves, slow-moving baroclinic waves and coastally trapped waves (Huthnance, 1978; Ezer, 2016; Hughes et al., 2019). Variations in the GS flow and path have a wide range of time scales: daily, mesoscale, seasonal, interannual, decadal and multidecadal or even longer. However, since direct continuous observations of the GS are relatively short, about 3 decades of satellite altimeter data and about 4 decades of cable observations of the Florida Current (Baringer and Larsen, 2001; Meinen et al., 2010), it is difficult to study past decadal and multidecadal variability in ocean dynamics and compare it to current and future climate change. For example, limited past temperature and salinity ship

observations and simple diagnostic numerical ocean models suggested that a dramatic decline of ~30% in the GS transport happened between the 1960s and 1970s (Levitus, 1989, 1990; Greatbatch et al., 1991); at the same period, an increase in sea level along the U.S. East Coast of 5-10 cm was observed (Ezer et al., 1995). These changes in the 1960s and 1970s resemble recent changes (i.e., coastal sea level rise during periods of GS weakening), but direct observations of the GS and AMOC were not available at the time, to allow comparisons with recent changes. Using ocean models forced by surface observations since the 1960s Blaker et al. (2014) found similarities between the extreme minimum in AMOC in 2009/2010 and a similar minimum in 1969/1970, but this approach has some shortcomings due to models' errors and lack of accurate surface forcing for earlier years.

One approach to overcome the above limitations of studying long term past changes, is to take advantage of the global coverage of recent altimeter data and combine this data with sparse, but long, tide gauges, to obtain global sea level reconstructions. Various optimization and spatial analysis methods were used to produce global reconstructed sea level (Church et al., 2011; Calafat et al., 2014; Hamlington et al., 2014; Hay et al., 2015; Dangendorf et al., 2019). Here, we used the latest hybrid reconstruction of Dangendorf et al. (2019) (see more details in the next section), since it contains both, spatial and temporal variability, as well as long term trends in sea level. Note that this monthly global reconstruction excludes non-climatic land motion, excludes seasonal cycles and is currently available at 1°×1° resolution for 1900-2015 (future improvements with assimilating higher resolution ocean models, newly digitized tide gauge data and an extended period are planned). Dangendorf et al. (2019) used this reconstruction to study global sea level acceleration and the influence of southern hemisphere winds on sea level, while Gehrels et al. (2020) used it to study past sea-level rise hotspots along the western North Atlantic Ocean coasts and their relation to the North Atlantic Oscillation (NAO) and to Arctic ice melt. The main goal here is to evaluate the usefulness of this reconstruction to study processes of long-term regional ocean dynamics. The western North Atlantic Ocean was chosen as a test case because of the important role that the GS and AMOC play in the basin's dynamics and the fact that the nearby coasts are considered "hotspots" for sea level rise, as described above. Some questions that the study addresses include: 1. Can a coarse resolution reconstruction that does not resolve sharp fronts like that of the GS be able to capture dynamic variations in a western boundary current? 2. How well does the reconstruction, which relies on a relatively short period of altimeter data and sparse tide gauge data, compare with recent independent observations of Atlantic Ocean circulation features such as the AMOC and the Florida Current? 3. What characterizes the long-term variability of sea level and ocean dynamics

and how do recent changes such as weakening AMOC compare with past changes? (are recent changes unprecedented, or more likely natural modes comparable to past changes over the last century?).

The paper is organized as follows: first, the data and the analysis methods are described in section 2, then in sections 3 the regional and global trends are compared, the reconstruction is evaluated against observations and decadal variations are studied, finally, in section 4, summary and conclusions are offered.

2. Data sources and analysis methods

The global reconstructed sea level (RecSL) record (1900-2015) analyzed here is described by Dangendorf et al. (2019). This RecSL is a hybrid reconstruction based on 479 tide gauge records, satellite altimeter data, and several geophysical ancillary datasets of contributing processes (e.g. gravitational, rotational, and deformational effects of mass changes known as "fingerprints", ocean circulation models and GIA), combining the techniques of the Kalman Smoother (Hay et al., 2015), optimal interpolation and empirical orthogonal functions (Calafat et al., 2014) at different timescales. The result is a monthly sea level field on a (1°×1°) grid that includes both variability and trends (though the annual cycle was removed). The aim here is to examine this global data set for its usefulness in studies of regional ocean dynamics. The western North Atlantic region is characterized by strong mesoscale variability, an intense western boundary current (the Gulf Stream) and important coastal impacts from climate change and sea level rise along the U.S. East Coast. Therefore, it is a challenging task for a coarse resolution reconstruction, which does not resolve mesoscale features, to accurately represent the regional dynamics. Fig. 1 shows for example, a comparison between the mean sea surface height (SSH) in the RecSL and the higher resolution (1/4°×1/4°) AVISO satellite altimeter data (Ducet et al., 2000). While the RecSL captured the main circulation patterns in the North Atlantic Ocean, the coarse resolution reconstruction is more noisy and underestimate spatial SSH gradients (note however, that fronts in each monthly field are more defined than in the long-term mean field).

From the reconstructed sea level, a proxy of the GS strength was derived for two regions (Fig. 1a). Based on the assumption that the surface flow is close to geostrophic balance, the sea level gradient across the GS represents the strength of the surface GS. A shortcoming of this proxy is that it may not capture subsurface changes. In the Mid-Atlantic Bight (MAB), for each longitude the GS location is defined by the maximum north-south sea level gradient, so the averaged maximum gradient represents

134 the mean eastward flowing GS in the region (58°W-70°W, 36°N-40°N). The units are change in cm per
135 1° latitude. In the South-Atlantic Bight (SAB) similar latitudinal averaging of east-west gradients will
136 represent the mean northward flowing GS in the region (76°W-80°W, 28°N-32°N), i.e., between the
137 Florida Strait and Cape Hatteras. These two proxies will be referred to as GS-MAB and GS-SAB,
138 respectively.

139 The monthly mean sea-level record (1927-2015) for the tide gauge station in Sewells Point near
140 Norfolk (76.33°W, 36.95°N; Fig. 1b) was obtained from the Permanent Service for Mean Sea-level
141 (PSMSL, www.psmsl.org; Woodworth and Player, 2003; Holgate et al., 2013). Since the RecSL record
142 does not include seasonal variability (Dangendorf et al., 2019), the mean annual cycle was calculated
143 and removed from the tide gauge data, to allow a fair comparison. The Norfolk station at the southern
144 end of the Chesapeake Bay was chosen because it is one of the U.S. cities currently facing some of the
145 largest impacts of sea level rise and increased flooding. This tide gauge record was subject to numerous
146 studies that link coastal sea level there with changes in ocean dynamics (Ezer, 2001, 2013; Ezer and
147 Corlett, 2012; Ezer et al., 2013; Ezer and Atkinson, 2014). While this tide gauge was part of the
148 reconstruction, so it is not completely independent from RecSL, the hybrid reconstruction has been
149 validated thoroughly using random independent unassimilated sites (see supplementary material in
150 Dangendorf et al., 2019). There are so many tide gauges along the U.S. East Coast that the
151 inclusion/exclusion of a single site such as Sewells Point will have a negligible effect on the
152 reconstructed fields.

153 The Atlantic Meridional Overturning Circulation (AMOC) data was obtained from the RAPID
154 observations at 26.5°N for 2005-2015, as described in various studies (https://www.rapid.ac.uk/;
155 McCarthy et al., 2012; Srokosz et al., 2012; Smeed et al., 2014, 2018). The AMOC transport (given in
156 Sverdrup; 1 Sv = 10^6 m^3 s^{-1}) is the sum of three components: 1. The upper mid-ocean transport obtained
157 from observations of density changes across the Atlantic Ocean, 2. The Ekman transport estimated from
158 wind stress data, and 3. The Gulf Stream transport obtained from cable measurements of the Florida
159 Current across the Florida Strait. These three components of AMOC are provided twice-daily, but they
160 were used here only to calculate monthly averages.

161 The annual Atlantic Multi-decadal Oscillation (AMO) index (Enfield et al., 2001) for 1900-2015
162 was obtained from NOAA (https://www.esrl.noaa.gov/psd/data/timeseries/AMO/); AMO represents
163 variations in the sea surface temperature (SST) over the Atlantic Ocean. Long-term variations in sea
164 level, such as a ~60-year long cycle, are thought of being influenced by AMO (Chambers et al., 2012)

and correlations of AMO with patterns of sea level along the U.S. and European coasts are often indicated (Ezer et al., 2016; Han et al., 2019).

Daily observations of the Florida Current (FC) transport at ~27°N (see Fig. 1b) for 1982-2015 were obtained from NOAA/AOML (www.aoml.noaa.gov/phod/floridacurrent/); the data is described by Baringer and Larsen (2000), Meinen et al. (2010) and many other studies. Monthly averaged values were calculated to allow comparisons with the RecSL record. Note that the FC data had a gap from October 1998 to June 2000. However, the EMD analysis as a sifting/filtering process (described below) can easily handle uneven sampling intervals and data gaps, so it can detect variations on time scales longer than the gaps- this has been experimentally tested for long tide gauge records (see Fig. 8 in Ezer et al., 2016).

A useful tool to analyze non-linear time series is the Empirical Mode Decomposition (EMD (Huang et al., 1998; Wu et al., 2007), where a repeated sifting process decomposes records into a finite number of intrinsic oscillatory modes $c_i(t)$ and a residual "trend" $r(t)$. The number of modes depends on the record length and the variability of the data. Unlike regression fitting methods, the shape of the trend is not predetermined (i.e., the method is "non-parametric"). Each individual mode does not necessarily represent a particular physical process, but often a group of modes can be shown to relate to a known forcing (Ezer et al., 2013; Ezer, 2015). The EMD decomposes the original time series into modes

$$\eta(t) = \sum_{i=2}^{N-1} c_i(t) + r(t). \quad (1)$$

In the EMD analysis output, mode-1 will be the original time series (η), modes 2 to N-1 are oscillating modes with different frequencies from high to low and mode-N will be the trend (r). Combining several low-frequency modes will be equivalent to a low-pass filter. Note that unlike spectral analysis, the frequency and amplitude in each mode is not constant, thus the analysis can capture non-linear changes, such as climatic changes in the amplitude of decadal variability. An improved version of the original EMD, is the Ensemble EMD (EEMD; Wu and Huang, 2009) used here, where ensemble of simulations with white noise are averaged. Here, 100 ensemble members are used with white noise of 0.1 of the standard deviation (see Ezer and Corlett, 2012 and Ezer et al., 2016, for sensitivity experiments with EEMD parameters and error estimations). The EEMD filters out unphysical modes and is more accurate for detecting real low frequency variability (Kenigson and Han, 2014). All the calculations here use the EEMD, though for simplicity the text refers to "EMD". Note that the sum of the low frequency modes plus the trend will be equivalent to a low-pass empirical filter that will have a lower number of degrees

of freedom than the original time series. Therefore, when calculating confidence levels on correlations between EMD modes, the "effective sampling size" or "effective number of degrees of freedom" is estimated following the method suggested by Thiebaux and Zwiers (1984). In this method, autocorrelation is used to estimate the typical time scales of low frequency EMD modes and then the confidence level is adjusted accordingly. Empirical testing showed for example that if for the 116-year long monthly RecSL record correlation coefficient of R=0.08 provides 95% confidence level ($P \leq 0.05$), to obtain the same confidence level for low frequency modes with autocorrelation time scales of 2, 5 and 10 years, will require $R >$ 0.25, 0.35 and 0.55, respectively. There have been discussions on the robustness of the EMD in terms of accurately detecting multi-decadal variability and non-linear trends in sea level records (Chambers, 2015). Therefore, to bolster the EMD based correlation analyses between the GS proxy, FC transport and the AMO, we also applied a wavelet coherence analysis (Grinsted et al., 2004), with the results being presented in the Supplementary Material.

3. Results

3.1. Regional and global sea level rise

Using the same reconstruction (RecSL) analyzed here, Dangendorf et al. (2019) found besides substantial decadal variability a significant and persistent acceleration in global mean sea level rise since the 1960s. They attributed the initiation of this recent acceleration to shifts in Southern Hemispheric wind patterns driving changes in ocean circulation increasing the ocean's heat uptake. In the western North Atlantic, some studies suggest that acceleration in sea level along the eastern coasts of North America may be related to a slowdown of AMOC and the GS (Leverman et al., 2005; Boon, 2012; Ezer and Corlett, 2012; Sallenger et al., 2012; Yin et al., 2013; Caesar et al., 2018). Future projections from climate models consistently indicate a weakening AMOC (Cheng et al., 2013; Reintges et al., 2017), though with divergent associated sea level responses in different models (Little et al., 2019). Therefore, it is important to understand the AMOC-sea level connection and try to detect current and past changes from observations. Bingham and Hughes (2009), for example, suggested that each 1 Sv weakening in AMOC could raise sea level along the North America coast by ~2 cm. To evaluate regional patterns in sea level rise, the sea level change in the southwestern North Atlantic for different periods was calculated (Fig. 2a-e) as well as the sea level change for the entire record 1900-2015 (Fig. 2f). Two

findings emerge from this analysis: First, sea level is rising at very different rates during different periods, for example, from 1915 to 1935 (Fig. 2a) sea level rose in the southwestern North Atlantic region by ~0.02-0.04 m (rate of ~1-2 mm/y; similar to the global rate seen in Fig. 2 of Dangendorf et al., 2019), while from 1995 to 2015 (Fig. 2e) sea level in this region rose by ~0.05-0.2 m (rate of 2.5-10 mm/y). Therefore, there is clearly a faster sea level rise since the 1990s compared with previous periods (i.e., sea level rise acceleration), but the sea level rise is spatially very uneven (Fig. 2f). It also seems that due to decadal variability, some periods experienced even decreasing rate of sea level rise (i.e., deceleration), for example, sea level rise from 1955 to 1975 (Fig. 2c) was slower than sea level rise from 1935-1955 (Fig. 2b). Second, the largest changes are seen near the GS around 35°N-40°N with additional changes on the rim of the subtropical gyre (reduction in sea level difference between the center and edge of the subtropical gyre can be interpreted as a sign of weakening circulation). The total sea level change between the first and last 5 years of the RecSL record (Fig. 2f) shows a faster sea level rise north of the GS (red area) and a slower sea level rise south of the GS (blue area), thus indicating a potential weakening trend in the geostrophic surface flow of the GS- this prospect is investigated later. Variations in the NAO and AMOC can cause changes in the GS position and/or in broadening its front (Taylor and Stephens, 1998; Joyce et al., 2000; Smeed et al., 2018), which can also result in spatial variations in sea level rise as seen here. However, the 1°×1° RecSL grid will not resolve most of the variability in the GS position (Fig. 1a), which nevertheless can be seen by the higher resolution altimeter data (Fig. 1b; see also Fig. 1 in Ezer et al., 2013).

A comparison of the global monthly mean sea level with the regional mean sea level in the southwestern North Atlantic (the area shown in Fig. 2) indicates a similar general trend (Fig. 3a), but a much larger interannual and decadal regional variability of up to ±4 cm over the global mean sea level (Fig. 3b). Regionally lower than average sea level is seen in the 1920s-1940s and higher than average sea level is seen in the 1950s and 1980s. Low-passed filtered data (Fig. 3b) show variations on two major time-scales, periods of ~5-10 years (the sum of EMD modes with periods longer than ~5 years is shown in red) and ~10-60 years (the sum of EMD modes with periods longer than ~10 years is shown in blue). The decadal and multidecadal variations in the global acceleration/deceleration of sea level were described by Dangendorf et al. (2019) and others, but we further want to evaluate here if regional variations in ocean dynamics may play a role and how these variations are connected to basin-scale climate modes (Han et al., 2019). Note that multidecadal modes are not resolved by the satellite altimetry era, so low-frequency variations in the hybrid RecSL record are estimated by the Kalman

Smoother applied on the tide gauge records while altimeter data contributing mostly to interannual to decadal variability (Dangendorf et al., 2019). We will return later to discuss the potential mechanisms behind the regional variability seen in Fig. 3b, but before that it is important to validate the RecSL record and evaluate its ability to capture observed the variability.

3.2. Comparison of the reconstruction with recent data

Very few data sets are long enough to evaluate the entire 116 years of the reconstruction. However, various recent observations can be used to examine how well the global reconstruction can resolve regional and basin-wide dynamic processes. The focus here is on two types of observations: coastal sea level and the Florida Current.

3.2.1 Coastal sea level

The long tide gauge record (starting in 1927) at Sewells Point in Norfolk, VA (in the lower Chesapeake Bay) has been the subject of many studies due to the acceleration in flooding at this city (Boon, 2012; Ezer and Corlett, 2012; Ezer, 2013; Ezer and Atkinson, 2014); this location can be used to represent sea level variability in the MAB (Ezer et al., 2013). Note that due to the coarse resolution, the reconstruction completely omits the Chesapeake Bay. The reconstructed sea level also removes land subsidence, which is substantial in Norfolk (Boon, 2012; Ezer and Corlett, 2012; Kopp, 2013). Moreover, the altimeter data that was used in the reconstruction do not extend to the near coast area or to rivers and bays, so that comparisons between tide gauge data and altimeter data often show that small-scale and high frequency variations in coastal sea level are not well represented in altimeter data, but interannual and decadal variations are captured quite well (e.g., see Fig. 2 in Ezer, 2015). Therefore, a comparison of this tide gauge with the reconstruction (basically a 1°×1° box offshore the Chesapeake Bay) will indicate what portion of the coastal sea level variability has origin in the offshore large-scale dynamic variability. Fig. 4 shows that while interannual variations in the reconstruction are highly correlated with the tide gauge, variability in the reconstruction is only about one half of the coastal observations. The correlation of ~0.8 is generally consistent with comparisons made by Dangendorf et al. (2019) for other locations and may indicate that about 60% of the coastal sea level variability is not locally generated within the Bay area (at least for monthly data- hourly or daily data may have more influence from local atmospheric forcing and tides). The reconstruction may not evenly represent all time scales, so to examine this point the variability in the coastal sea level and in the reconstructed sea level are decomposed into EMD

modes (Fig. 5). Cross-correlations help to identify the main oscillations in each mode. While statistically significant correlation (at 95% confidence) is found at all modes (see section 2 for details on confidence levels of EMD modes), the amplitudes of the variations are underestimated for high frequency oscillations. In Fig. 6 the EMD modes of the observed and reconstructed sea level are compared. While the reconstruction captured almost perfectly the mean frequency of each observed mode (Fig. 6a), the variability of the reconstruction is underestimated by about a factor of two for the whole time series (mode 1) and for oscillations with periods T<~5 years (Fig. 6b). The underestimation is likely due to the variability in the satellite altimeter data and not due to the reconstruction itself. For longer time scales (modes 7-10) the reconstruction captured the coastal variability extremely well with correlations of ~0.9-1. The lowest frequency of oscillating mode 10 in Fig. 5 is almost identical in the reconstructed and observed sea level, showing an apparent positive acceleration in sea level rise since the 1960s, in accordance with the global acceleration seen in Dangendorf et al. (2019). Modes 6-8 (with periods of 5-20 years) show especially strong oscillations (Fig. 5 and Fig. 6c). Note that much longer records are needed to study the oscillations of the lowest frequencies when only a few cycles are available, though unlike spectral analysis methods, the EMD method is able to detect the potential existence of very low frequency modes from even incomplete cycles.

3.2.2 The Florida Current (FC)

In Fig. 7 the observed FC transport for 1983-2015 is compared with the reconstructed GS proxy for the MAB and the SAB. Note that for this period, the FC shows a small weakening trend of -0.03 Sv/yr (~0.9%/decade), while a larger recent weakening (~1.5%/decade) is seen during the RAPID/AMOC observations of 2005-2015 (see discussion in next section). The correlations of the FC with the GS proxy are larger in the SAB (R=0.58; Fig. 7b) where the GS is closer to the Florida Straits than in the MAB (R=0.28; Fig. 7a) where the GS is farther downstream from the observed FC (see Fig. 1). The lower correlation in the MAB (though statistically significant at 95%) seems due to a phase lag between the upstream SAB and the downstream MAB. This incoherence between the GS and coastal sea level on the two sides of Cape Hatteras (i.e., the SAB versus the MAB) was investigated in several recent studies (Woodworth et al., 2016; Valle-Levinson et al., 2017; Domingues et al., 2018; Ezer, 2019). It is interesting to note that the relation between low frequency changes in the FC transport and sea level as seen in Fig. 7b implies a ratio of about 1 Sv to 1.5 cm while Bingham and Hughes (2009) suggested a ratio of ~1 Sv to 2 cm between AMOC transport and coastal sea level.

EMD analysis further compares relationship between the GS-SAB proxy (derived from east-west sea level difference) and the observed FC for different modes (Fig. 8). The high frequency oscillations of the FC and the GS-SAB are not significantly correlated, in fact, oscillations at ~2-year period show a small but non-significant anticorrelation at lag zero (second panel in Fig. 8). However, variability on time scales larger than ~5 years are highly correlated (R=0.8-0.9 for modes 6-8 in Fig. 8) with the GS-SAB lagging behind the observed FC transport; this low frequency variability in modes 6-8 represents cycles with periods of ~5 years, ~12 years and ~24 years, respectively (see right panels in Fig. 8). This result is further supported by a complementary wavelet coherence analysis (Supplementary Fig. S1). While theoretically it is expected that sea level difference across the GS will be correlated with the FC, it is encouraging that a coarse resolution global reconstruction on a 1-degree grid that does not resolve the GS front very well can still capture the majority of the low frequency variability of the FC. It is noted that although the reconstruction is based on satellite altimeter data that started in 1993, ocean dynamic variability in the 1980s, before the satellite age, is still captured quite well.

3.3. Potential driving mechanisms for decadal variability in the RecSL

Variability in the GS-MAB proxy (obtained from sea level gradients as described in section 2) is shown in Fig. 9a, indicating large variability on interannual and decadal time scales with a persistent weakening trend since ~1990, after a period of strengthening flow from the 1970s to the 1990s. The changes in the low-frequency oscillations are shown in Fig. 9b, indicating two long periods with declining GS strength (red area) during the 1960s and 1970s and after ~1995, with maximum weakening of ~25% per decade. Recent observations by Andres et al. (2020) at 68.5°W found the GS transport to be about 10% weaker today than it was in the 1980s at the same location, but the same study also found very large discrepancy in the trend between two sections located just a few 100 km from each other, a western section from ship crossing showed no statistically significant trend (Rossby et al., 2014) and an eastern section from mooring data showed potential weakening of ~5-10% per decade. Based on altimeter data, Dong et al. (2019) and Zhang et al. (2020) also showed different trends between the eastern and western parts of the GS. Therefore, average GS proxy over a large area as done here may filter out spatial variations; the RecSL record is also much longer than the altimeter data used in the above studies. The coarse resolution of the reconstruction also served as a filter that smoothed out small spatial variations and the impact from local recirculation gyres as seen in Andres et al. (2020). The GS-MAB proxy here shows that the recent weakening period is the longest in this record. To test if the long period of GS weakening

is "unprecedented" or distinct from random natural variability, statistical analysis with 1000 simulations using random red noise (following an autoregressive process of the order 1) imitating the spectrum of the record in Fig. 9a was performed and the results are shown in Supplementary Fig. S2. This analysis shows that obtaining long periods of weakening from random variability is extremely rare: in 116,000 years of artificial simulations there were only 3 cases of weakening of 10%/decade that lasted for 10 years. For comparison, in the 116 years of reconstructed GS there were 2 such cases, with 10%/decade weakening of ~10 years in the 1970s and ~15 years in the 2000s.

Various mechanisms can affect variations in the GS flow such as changes in the strength of the subpolar gyre circulation (Hakkinen and Rhines, 2004) or weakening in the AMOC (Bryden, 2005; McCarthy et al., 2012; Srokosz et al., 2012; Ezer et al., 2013; Smeed et al., 2014, 2018; Blaker et al., 2014; Roberts et al., 2014; Ezer, 2015; Rahmstorf et al., 2015; Caesar et al., 2018). The earlier period of GS weakening in the 1960s-1970s is consistent with observations and models that showed large density changes in the North Atlantic and as much as 30% weakening in the GS between 1955-1959 and 1970-1974 (Levitus, 1989, 1990; Greatbatch et al., 1991; Ezer et al., 1995). At the time of these early studies, before the age of satellite altimeters, observations were limited and models less sophisticated, so there were some doubts that the large weakening in the GS during the 1960s and 1970s was real. However, this reconstruction by Dangendorf et al. (2019) and another reconstruction of AMOC from sea level data by Ezer (2015) both confirm the results of the early studies, showing only two periods of pronounced weakening AMOC since the 1950s. Future observations will show if the recent decline is just a relaxation from the strong GS of the 1980s and 1990s or a continuous downward trend. The relation between the GS-MAB proxy and basin-scale processes are thus analyzed below by looking at two measures, AMO and AMOC.

3.3.1 The Atlantic Multi-decadal Oscillation (AMO)

The large decadal and multidecadal variations in the GS-MAB proxy as seen in Fig. 9 are compared with the annual Atlantic Multi-decadal Oscillation index (AMO; Enfield et al., 2001) for 1900-2015 (Fig. 10). EMD is used to compare oscillating modes with similar time scales. Hi-frequency modes of the GS and AMO are not significantly correlated, but variability in the two time series on time scales of ~10-60 years are correlated, especially the lowest frequency modes (bottom two panels in Fig. 10), with correlations of 0.5-0.8 that are statistically significant at 95% (after considering the reduction in degrees of freedom in the low-frequency modes, see explanation in section 2). The wavelet coherence analysis

(Supplementary Fig. S3) principally confirms the sign of these correlations in a 16-year frequency band, though they are not statistically significant. This indicates that the correlations identified by the EMD should be taken as preliminary, requiring further data and analyses that are beyond the scope of this paper. Mode 6 (bottom panel in Fig. 10) indicates cyclic behavior at periods up to ~60 years, consistent with previous studies (Chambers et al., 2012). Various studies indicated a connection between AMO, which represents variations in SST, and sea level. Ezer et al. (2016) for example, showed a change in the sign of the correlation across the GS, which could indicate changes in the GS strength; if sea level rises at one side of the GS and drops at the other side, the change in gradient indicates a change in strength or position of the GS. The EMD analysis also indicates non-stationary variations with changing amplitude and period over time, showing larger oscillations in all modes after the 1960s, though this might also be related to a decreasing performance in the sea level reconstruction before the 1940s, when the tide gauge records become much sparser. It is acknowledged that correlation does not indicate cause-and-effect and that each EMD mode may not necessarily represent a specific mechanism. For example, for oscillations on time scales of 10-40 years AMO lags behind the GS by 2-5 years (the 2nd and 3rd panels in Fig. 10), but for longer time scales (bottom panel of Fig. 10) the GS lags behind the AMO by 5-10 years. It is interesting to note that modes 4 and 5 captured the minimum GS-MAB in the 1970s, while mode 6 captured the minimum in the 2000s. The positive correlation between low frequency variations in the GS and the AMO can be interpreted in several ways- during periods of more intense flow the GS transports more heat to the North Atlantic, thus raising SST and increasing the AMO index (i.e., AMO lags behind the GS), but on the other hand, the AMO is connected to slow variations in AMOC that after some delay can impact the GS (i.e., GS lags behind AMO). The low frequency multidecadal modes seen here resemble findings from ocean models such as the decadal variations seen in the early Atlantic model of Ezer (1999) and in a realistic Atlantic Ocean model of Sevellec and Federov (2013), who found an oscillatory AMOC mode with a period of ~24 years and an e-folding decay time scale of ~40 years that relates to westward propagation of large-scale temperature anomalies (thus connecting AMOC with the AMO). Therefore, the relation of GS-MAB and the observed AMOC is analyzed next.

3.3.2 The Atlantic Meridional Overturning Circulation (AMOC)

Continuous observations of AMOC transport at 26.5°N are available since 2004 from the RAPID program (McCarthy et al., 2012; Srokosz et al., 2012; Baringer et al., 2013; Smeed et al., 2014, 2018).

Previous studies found connections between AMOC and sea level difference across the GS as derived from two tide gauges (Ezer, 2015), so it is interesting to examine if the reconstructed GS shows relation to the observed AMOC. The RAPID/AMOC transport is the combined contribution from three sources, Upper Mid-Ocean (UMO) due to density gradients, wind-driven Ekman (EK) transport and Gulf Stream transport as observed by the cable across the Florida Current (FC). These three components and the total AMOC transport are compared with the proxy GS-MAB record for 2005-2015 (Fig. 11). Shown are the monthly values and the low frequency EMD modes. The low frequency variations in the total AMOC transport are significantly correlated (P<0.05) with the GS-MAB proxy (R=0.64) and both show a weakening trend of ~12% over this decade of comparison (Fig. 11a). However, the GS-MAB proxy is not significantly influenced by the EK (Fig. 11c; R=0.1) or the FC (Fig. 11d; R=-0.1) components of AMOC. Note that the FC record used by RAPID in Fig. 11d is much shorter than the entire FC record in Fig. 7, thus the longer record captures lower frequency modes and shows higher correlation with the GS-MAB (Fig. 7a; R=0.28). It does seem though that more than 50% of the variability in the GS-MAB is due to the UMO (R=0.72). Moreover, the weakening trend in the GS-MAB also seems to be due to the weakening in the UMO (Fig. 11b). The GS-MAB lags by about a year behind changes in the UMO, a result also obtained in Ezer (2015). Coherent oscillations with periods of ~2-3 years dominate the low-frequency modes for GS-MAB, UMO, EK and the total AMOC transport. In summary, it is encouraging that despite the limitation of using only surface and coastal data in the reconstruction, it can capture the variability of AMOC including changes in the subsurface density field (i.e., UMO). It is also noted that in the earlier period of weakening GS in the 1970s (Fig. 9), changes in the Atlantic density field rather than changes in the wind fields were suggested as the main cause of this weakening (Levitus, 1989, 1990; Greatbatch et al., 1991; Ezer et al., 1995), which is consistent with the finding here of the main cause of the recent period of GS weakening.

4. Summary and conclusions

Since continuous coverage of global sea level from satellite altimeters started only in recent decades (since the middle 1990s), and century-long tide gauge records are sparse, it is a challenge to study long-term variations in sea level and ocean dynamics (decades to multi-decades and longer) with existing data. Such studies are important for understanding natural variations, anthropogenic changes, and the increased risk to coastal communities from climate change and sea level rise. To overcome the lack of

past data and sparse tide gauges data, various statistical optimization techniques were used to reconstruct past global sea level. Here, a new hybrid reconstruction by Dangendorf et al. (2019) for 1900-2015 was examined, with two main goals in sight: first, to evaluate the reconstruction against recent observations in order to see if the global coarse resolution reconstruction can capture variations in regional coastal sea level and ocean dynamics and second, to study mechanisms and forcing of long term variability and their relation to basin scale modes. The focus of the study was on the southwestern North Atlantic Ocean, where the dynamics are dominated by the variability of the Gulf Stream system, and where offshore GS dynamics can drive coastal sea level rise and variability (Blaha, 1984; Leverman et al., 2005; Ezer, 2001, 2013, 2015, 2019; Ezer et al., 2013; Salenger et al., 2012; Yin et al., 2013; Domingues et al., 2018).

Close examination of the western North Atlantic region in the reconstructed sea level shows uneven acceleration at different periods during the 116-year record, with larger acceleration in the last two decades than that of previous periods, as indicated globally in Dangendorf et al. (2019) and others. However, regionally, the largest changes in sea level rise rates are found near the GS with often opposing sea level changes north and south of the GS front, thus pointing to the hypothesis that spatial variations in sea level near the GS are linked to changes in the GS strength (and possibly position). To study variations in the GS, a proxy of the GS strength was derived from sea level differences across the GS in two subregions, the SAB and the MAB. Using EMD analysis, long-term (time scales longer than 5 years) variations in the reconstructed GS were found to be significantly correlated with the low frequency oscillations of the AMO, detecting the two periods of weakening GS. Calculations using wavelet coherence found similar patterns as the EMD calculations, but the correlations were not statistically significant (Supplementary material). Another interesting result is that during the 116-year record, there are two distinct periods of relatively long weakening in the GS flow, each one lasts for at least a decade when the maximum trend was a declining flow of about 20-25% per decade. The first period with a slowing down GS was seen in the 1960s and 1970s. This period of weakening circulation was previously identified by limited observations (Levitus, 1989, 1990) and early basin-scale diagnostic models (Greatbatch et al., 1991; Ezer et al., 1995) that suggested up to 30% slowdown in the GS transport over a 15-year period (though model results could not be verified due to lack of observations at the time). This weakening was suggested to relate mostly to changes in the subsurface Atlantic Ocean density field and to lesser degree to changes in the wind-driven Ekman transport. Regional acceleration in sea level rise along the U.S. East Coast due to the weakening GS was also seen in models and data

during this time (Ezer et al., 1995). However, only years later, based on more data, the link between weakening in the GS and AMOC and accelerated coastal sea level became a topic of considerable research (e.g., Levermann et al., 2005; Yin et al., 2010; Sallenger et al., 2012; Ezer et al., 2013). The second period of significant weakening in the reconstructed GS, was the longest in the 116-year record (~1998-2015; it may continue beyond the reconstruction record). It is noted though that the uncertainties of the reconstruction increase substantially before the 1950s, when tide gauge records become sparse. Experiments with 1000 simulations of red noise (Supplementary material) show that obtaining such a long period of GS weakening from random natural variability is extremely rare. During the more recent period significantly more observations exist that support the recent weakening trend, including altimeter data (Ezer et al., 2013; Ezer, 2015; Dong et al., 2019; Zhang et al., 2020), reconstruction from temperature data (Rahmstorf et al., 2015; Caesar et al., 2018) direct measurements of the GS (Rossby et al., 2014; Andres et al., 2020) and the AMOC/RAPID observations (McCarthy et al., 2012; Srokosz et al., 2012; Baringer et al., 2013; Smeed et al., 2014). A comparison of the reconstructed GS and the observed AMOC shows a similar downward trend for 2005-2015 and similar oscillations with periods of 2-5 years. The recent weakening of the reconstructed GS and the variability were correlated with variations in the upper mid-ocean transport component of AMOC and to lesser degree in recent years by changes in the Ekman transport, somewhat resembling processes suggested in the past to explain the 1960s-1970s changes.

While Dangendorf et al. (2019) validated the RecSL globally, another goal here was to evaluate the reconstructed sea level against recent observations in the study area. Coastal tide gauge data in the lower Chesapeake Bay (in the flood prone city of Norfolk) for 1927-2015 were compared with the reconstructed sea level offshore (the Bay is completely absent from the 1°×1° coarse resolution reconstruction). Observations of the Florida Current transport for 1982-2015 were also compared with the reconstructed GS in the SAB. EMD analysis (Huang et al., 1998) was used to decompose the time series into non-stationary modes of different time-scales in order to examine what portion of the observed variability can be captured by the reconstruction. The results show that for time scales of ~5-year and longer, the reconstruction can capture most of the observed variability (correlations of 0.8-0.9) in both, the coastal sea level and the FC transport. Wavelet coherence analysis of the FC and GS-SAB (Supplementary material) largely confirms the results of the EMD analysis.

In summary, the study demonstrated that despite the coarse horizontal resolution of the global reconstruction (1°×1°), and the sparse data that was available before the satellite altimetry age, some

long-term variations in regional dynamics can be captured quite well by this global reconstruction, therefore providing a useful tool for studies of long-term past variability in other regions as well. The long reconstruction can help studies of decadal and longer natural variability as well as anthropogenic climate change. For example, the study shows that while the ocean circulation and the GS are subject to natural multidecadal variations, the recent weakening in the GS is unprecedented in its length during the 116 years of the reconstruction. It also confirmed the existence of another period of significant weakening GS during the 1960s and 1970s, which previously was suggested only by limited observations. Future observations are needed to determine if the recent weakening will last due to anthropogenic forces or recover, like the previous slowdown.

Acknowledgments: The study is part of Old Dominion University's Climate Change and Sea Level Rise Initiative at the Institute for Coastal Adaptation and Resilience (ICAR). Data used here are available from the following sites: PSMSL sea level (http://www.psmsl.org/), AVISO altimeter data (http://las.aviso.oceanobs.com), AMO index (https://www.esrl.noaa.gov/psd/data/timeseries/AMO/), AMOC transports from the RAPIC project (http://www.rapid.ac.uk/rapidmoc/) and FC transport from NOAA/AOML (www.aoml.noaa.gov/phod/floridacurrent/). The RecSL data is available by request from the authors. Many useful suggestions that helped to improve the manuscript were provided by Jenny Jardine, Tarmo Soomere, Christopher Piecuch and three anonymous referees.

References

Andres, M, Donohue, K. A., and Toole, J. M.: The Gulf Stream's path and time-averaged velocity structure and transport at 68.5°W and 70.3°W, Deep-Sea Res., 156, doi:10.1016/j.dsr.2019.103179, 2020.

Baringer, M. O., and Larsen, J. C.: Sixteen Years of Florida Current Transport at 27°N, Geophys. Res. Lett., 28(16), 3,179-3,182, doi:10.1029/2001GL013246, 2001.

Bingham, R. J., and Hughes, C. W.: Signature of the Atlantic meridional overturning circulation in sea level along the east coast of North America, Geophys. Res. Lett., 36, L02603, doi:10.1029/2008GL036215, 2009.

Blaha, J. P.: Fluctuations of monthly sea level as related to the intensity of the Gulf Stream from Key West to Norfolk, J. Geophys. Res., 89(C5), 8033-8042, doi:10.1029/JC089iC05p08033, 1984.

526 Boon, J. D.: Evidence of sea level acceleration at U.S. and Canadian tide stations, Atlantic coast, North
527 America, J. Coast. Res., 28(6), 1437-1445, doi:10.2112/JCOASTRES-D-12-00102.1, 2012.
528 Blaker, E. T, Hirschi, J. J. M, McCarthy, G., Sinha, B., Taws, S., Marsh, R., Coward, A., and de Cuevas,
529 B.: Historical analogues of the recent extreme minima observed in the Atlantic meridional
530 overturning circulation at 26°N, Clim. Dyn., doi:10.1007/s00382-014-2274-6, 2014.
531 Bryden, H. L., Longworth, H. R., and Cunningham, S. A.: Slowing of the Atlantic meridional
532 overturning circulation at 25°N, Nature, 438, 655-657, doi:10.1038/nature04385, 2005.
533 Caesar, L., Rahmstorf, S., Robinson, A., Feulner, G., and Saba, V.: Observed fingerprint of a weakening
534 Atlantic Ocean overturning circulation, Nature, 556, 191-196, doi:10.1038/s41586-018-0006-5, 2018.
535 Calafat, F. M., Chambers, D. P., and Tsimplis, M. N.: On the ability of global sea level reconstructions
536 to determine trends and variability, J. Geophys. Res., 119, 1572-1592, doi:10.1002/2013JC009298,
537 2014.
538 Cazenave, A., and Cozannet, G. L.: Sea level rise and its coastal impacts, Earth's Future, 2, 15-34, doi:
539 10.1002/2013EF000188, 2014.
540 Chambers, D. P.: Evaluation of empirical mode decomposition for quantifying multi-decadal variations
541 and acceleration in sea level records, Nonlin. Processes Geophys., 22, 157-166, doi:10.5194/npg-22-
542 157-2015, 2015.
543 Chambers, D. P., Merrifield, M. A., and Nerem, R. S.: Is there a 60-year oscillation in global mean sea
544 level?, Geophys. Res. Lett., 39, L18607, doi:10.1029/2012GL052885, 2012.
545 Cheng, W., Chiang, J. C., and Zhang, D.: Atlantic Meridional Overturning Circulation (AMOC) in
546 CMIP5 models: RCP and historical simulations, J. Clim., 26, 7187-7197, doi:10.1175/JCLI-D-12-
547 00496.1, 2013.
548 Church, J. A., and White N. J.: A 20th century acceleration in global sea-level rise, Geophys. Res. Lett.,
549 33(1), doi:10.1029/2005GL024826, 2006.
550 Church, J. A., and White N. J.: Sea-level rise from the late 19th to the early 21st century, Surv. Geophys.,
551 32, 585-602, doi:10.1007/s10712-011-9119-1, 2011.
552 Church, J. A., White, N. J., Konikow, L. F., Domingues, C. M., Cogley, J. G., Rignot, E., Gregory, J.
553 M., van den Broeke, M. R., Monaghan, A. J., and Velicogna, I.: Revisiting the Earth's sea-level and
554 energy budgets from 1961 to 2008, Geophys. Res. Lett., 38, L18601, doi:10.1029/2011GL048794,
555 2011.

556 Dangendorf, S., Rybski, D., Mudersbach, C., Müller, A., Kaufmann, E., Zorita, E., and Jensen, J.:
557 Evidence for long-term memory in sea level, Geophys. Res. Lett., 41, 5564-5571,
558 doi:10.1002/2014GL060538, 2014.
559 Dangendorf, S., Marcos, M., Wöppelmann, G., Conrad, C. P., Frederikse, T., and Riva, R.:
560 Reassessment of 20th century global mean sea level rise, Proc. Nat. Acad. Sci.,
561 doi:10.1073/pnas.1616007114, 2017.
562 Dangendorf, S., Hay, C., Calafat, F. M., Marcos, M., Piecuch, C. G., Berk, K., and Jensen, J.: Persistent
563 acceleration in global sea-level rise since the 1960s, Nat. Clim. Change, 9, 705-710,
564 doi:10.1038/s41558-019-0531-8, 2019.
565 Domingues, R., Goni, G., Baringer, N., and Volkov, D.: What caused the accelerated sea level changes
566 along the U.S. East Coast during 2010–2015?, Geophys. Res. Lett., 45, 13,367-13,376,
567 doi:10.1029/2018GL0811832018, 2018.
568 Dong, S., Baringer, M. O. and Goni, G. J.: Slow Down of the Gulf Stream during 1993–2016, Sci. Rep.,
569 9, 6672, doi:10.1038/s41598-019-42820-8, 2019.
570 Ducet, N., Le Traon, P. Y., and Reverdin, G.: Global high resolution mapping of ocean circulation from
571 the combination of T/P and ERS-l/2, J. Geophys. Res., 105(C8), 19,477-19,498,
572 doi:10.1029/2000JC900063, 2000.
573 Enfield, D. B., Mestas-Nunez, A. M., and Trimble, P. J.: The Atlantic Multidecadal Oscillation and its
574 relationship to rainfall and river flows in the continental U.S., Geophys. Res. Lett., 28: 2077-2080,
575 2001.
576 Ezer, T.: Decadal variabilities of the upper layers of the subtropical North Atlantic: An ocean model
577 study, J. Phys. Oceanogr., 29(12), 3111-3124, doi:10.1175/1520-0485(1999)029, 1999.
578 Ezer, T.: Can long-term variability in the Gulf Stream transport be inferred from sea level?, Geophys.
579 Res. Let., 28(6), 1031-1034, doi:10.1029/2000GL011640, 2001.
580 Ezer, T.: Sea level rise, spatially uneven and temporally unsteady: Why the U.S. East Coast, the global
581 tide gauge record, and the global altimeter data show different trends, Geophys. Res. Lett., 40, 5439-
582 5444, doi:10.1002/2013GL057952, 2013.
583 Ezer, T.: Detecting changes in the transport of the Gulf Stream and the Atlantic overturning circulation
584 from coastal sea level data: The extreme decline in 2009-2010 and estimated variations for 1935-
585 2012, Glob. Planet. Change, 129, 23-36, doi:10.1016/j.gloplacha.2015.03.002, 2015.

586 Ezer, T.: Can the Gulf Stream induce coherent short-term fluctuations in sea level along the U.S. East
587 Coast?: A modeling study, Ocean Dyn., 66(2), 207-220, doi:10.1007/s10236-016-0928-0, 2016.
588 Ezer, T.: Regional differences in sea level rise between the Mid-Atlantic Bight and the South Atlantic
589 Bight: Is the Gulf Stream to blame?, Earth's Future, 7(7), 771-783, doi:10.1029/2019EF001174,
590 2019.
591 Ezer, T., and Corlett, W. B., Is sea level rise accelerating in the Chesapeake Bay? A demonstration of a
592 novel new approach for analyzing sea level data, Geophys. Res. Lett., 39, L19605,
593 doi:10.1029/2012GL053435, 2012.
594 Ezer, T., and Atkinson, L. P.: Accelerated flooding along the U.S. East Coast: On the impact of sea-level
595 rise, tides, storms, the Gulf Stream, and the North Atlantic Oscillations, Earth's Future, 2(8), 362-382,
596 doi:10.1002/2014EF000252, 2014.
597 Ezer, T., Mellor, G. L., and Greatbatch R. J.: On the interpentadal variability of the North Atlantic
598 ocean: Model simulated changes in transport, meridional heat flux and coastal sea level between
599 1955-1959 and 1970-1974, J. Geophys. Res., 100(C6), 10,559-10,566, doi:10.1029/95JC00659,
600 1995.
601 Ezer, T., Atkinson, L. P., Corlett, W. B., and Blanco, J. L.: Gulf Stream's induced sea level rise and
602 variability along the U.S. mid-Atlantic coast, J. Geophys. Res., 118, 685-697,
603 doi:10.1002/jgrc.20091, 2013.
604 Ezer, T., Haigh I. D., and Woodworth, P. L.: Nonlinear sea-level trends and long-term variability on
605 western European coasts, J. Coast. Res., 32(4),744-755, doi:10.2112/JCOASTRES-D-15-00165.1,
606 2016.
607 Frederikse, T., Simon, K., Katsman, C. A., and Riva, R.: The sea-level budget along the Northwest
608 Atlantic coast: GIA, mass changes, and large-scale ocean dynamics, J. Geophys. Res., 122, 5486-
609 5501, doi:10.1002/2017JC012699, 2017.
610 Gehrels, W. R., Dangendorf, S., Barlow, N. L. M., Saher, M. H., Long, A. J., Woodworth, P. L.,
611 Piecuch, C. G., and Berk, K.: A preindustrial sea-level rise hotspot along the Atlantic coast of North
612 America, Geophys. Res. Lett., 47, doi:10.1029/2019GL085814, 2020.
613 Goddard, P. B., Yin, J., Griffies, A. M., and Zhang, S.: An extreme event of sea-level rise along the
614 Northeast coast of North America in 2009–2010, Nature Comm., 6, 6346, doi:10.1038/ncomms7346,
615 2015.

Greatbatch, R. J., Fanning, A. F., Goulding, A. D., and Levitus, S.: A diagnosis of interpentadal circulation changes in the North Atlantic, J. Geophys. Res., 96(C12), 22009-22023, doi:10.1029/91JC02423, 1991.

Grinsted, A., Moore, J. C., Jevrejeva, S.: Application of the cross wavelet transform and wavelet coherence to geophysical time series, Nonlin. Proc. Geophys., 11(5/6), 561-566, 2004.

Haigh, I. D., Wahl, T., Rohling, E. J., Price, R. M., Battiaratchi, C. B., Calafat F. M., and Dangendorf, S.: Timescales for detecting a significant acceleration in sea level rise, Nature Comm., 5, 3635, doi:10.1038/ncomms4635, 2014.

Hay, C. H., Morrow, E., Kopp, R. E. and Mitrovica, J. X.: On the robustness of Bayesian fingerprinting estimates of global sea level change, J. Clim., 30, 3025-3038, doi:10.1175/JCLI-D-16-0271.1, 2015.

Hakkinen, S., and Rhines, P. B.: Decline of subpolar North Atlantic circulation during the 1990s, Science, 304, 555-559, doi:10.1126/science.1094917, 2004.

Hamlington, B. D., Leben, R. R., Strassburg, M. W. and Kim, K.-Y.: Cyclostationary empirical orthogonal function sea-level reconstruction, Geosci. Data J., 1, 13-19, doi:10.1002/gdj3.6, 2014.

Han, W., Stammer, D., Thompson, P., Ezer, T., Palanisamy, H., Zhang, X., Domingues, C., Zhang, L., and Yuan, D.: Impact of basin-scale climate modes on coastal sea level: a review, Surv. Geophys., 40(6), 1493-1541, doi:10.1007/s10712-019-09562-8, 2019.

Holgate, S. J., Matthews, A., Woodworth, P. L., Rickards, L. J., Tamisiea, M. E., Bradshaw, E., Foden, P. R., Gordon, K. L., Jevrejeva, S., Pugh, J.: New data systems and products at the Permanent Service for Mean Sea Level, J. Coast. Res., 29(3), 493-504, doi: 10.2112/JCOASTRES-D-12-00175.1, 2013.

Huang, N. E., Shen, Z., Long, S. R., Wu, M. C., Shih, E. H., Zheng, Q., Tung, C. C., and Liu, H. H.: The empirical mode decomposition and the Hilbert spectrum for non stationary time series analysis, Proc. R. Soc. London, Ser. A, 454, 903-995, doi:10.1098/rspa.1998.0193, 1998.

Hughes, C. W., Fukumori, I., Griffies, S. M., Huthnance, J. M., Minobe, S., Spence, P., Thompson, K. R., and Wise, A.: Sea level and the role of coastal trapped waves in mediating the influence of the open ocean on the coast, Surv. Geophys., 40(6), 1467-1492, doi:10.1007/s10712-019-09535-x. 2019.

Huthnance, J. M.: On coastal trapped waves: Analysis and numerical calculation by inverse iteration, J. Phys. Oceanogr., 8, 74-92, doi:10.1175/1520-0485(1978)008<0074:OCTWAA>2.0.CO;2, 1978.

Jevrejeva, S., Moore, J. C., Grinsted, A., and Woodworth, P. L.: Recent global sea level acceleration started over 200 years ago?, Geophys. Res. Lett., 35, L08715, doi:10.1029/2008GL033611, 2008.

Joyce, T. M., Deser, C., and Spall, M. A.: The Relation between decadal variability of subtropical mode water and the North Atlantic Oscillation, J. Clim., 13, 2550-2569, 2000.

Kenigson, J. S., and Han, W.: Detecting and understanding the accelerated sea level rise along the east coast of US during recent decades, J. Geophys. Res., 119(12), 8749-8766, doi:10.1002/2014JC010305, 2014.

Kopp, R. E.: Does the mid-Atlantic United States sea-level acceleration hot spot reflect ocean dynamic variability?, Geophys. Res. Lett., 40(15), 3981-3985, doi:10.1002/grl.50781, 2013.

Levermann, A., Griesel, A., Hofmann, M., Montoya, M., and Rahmstorf, S., Dynamic sea level changes following changes in the thermohaline circulation, Clim. Dyn., 24(4), 347-354, doi:10.1007/s00382-004-0505-y , 2005.

Levitus, S.: Interpentadal variability of temperature and salinity at intermediate depths of the North Atlantic Ocean, 1970–1974 versus 1955–1959, J. Geophys. Res., 94, 6091-6131, doi:10.1029/JC094iC05p06091, 1989.

Levitus, S.: Interpentadal variability of steric sea level and geopotential thickness of the north Atlantic Ocean, 1970–1974 versus 1955–1959, J. Geophys. Res., 95(C4), 5233-5238, doi:10.1029/JC095iC04p05233, 1990.

Little, C. M., Hu, A., Hughes, C. W., McCarthy, G. D., Piecuch, C. G., Ponte, R. M., and Thomas, M. D.: The Relationship between U.S. East Coast sea level and the Atlantic Meridional Overturning Circulation: A review, J. Geophys. Res., 124, 6435-6458, doi:10.1029/2019JC015152, 2019.

McCarthy, G., Frejka-Williams, E., Johns, W. E., Baringer, M. O., Meinen, C. S., Bryden, H. L., Rayner, D., Duchez, A., Roberts, C., and Cunningham, S. A., Observed interannual variability of the Atlantic meridional overturning circulation at 26.5^{o}N, Geophys. Res. Lett., doi:10.1029/2012GL052933, 2012.

Meinen, C. S., Baringer, M. O., and Garcia, R. F.: Florida Current transport variability: An analysis of annual and longer-period signals, Deep-Sea Res., 57(7), 835-846, doi:10.1016/j.dsr.2010.04.001, 2010.

Merrifield, M. A., Merrifield S. T. and Mitchum, G. T.: An anomalous recent acceleration of global sea level rise, J. Clim., 22, 5772-5781, doi:10.1175/2009JCLI2985.1, 2009.

Montgomery, R. (1938) Fluctuations in monthly sea level on eastern U.S. coast as related to dynamics of western North Atlantic Ocean, J. Mar. Res. 1, 165-185, 1938.

Piecuch, C. G., Dangendorf, S., Gawarkiewicz, G. G., Little, C. M., Ponte, R. M., and Yang, J.: How is New England coastal sea level related to the Atlantic meridional overturning circulation at 26°N?, Geophys. Res. Lett., 46, 5351-5360, doi:10.1029/2019GL083073, 2019.

Rahmstorf, S., Box, J., Feulner, G., Mann, M. E., Robinson, A., Rutherford, S., and Schaffernicht, E. J.: Exceptional twentieth-century slowdown in Atlantic Ocean overturning circulation. Nature Clim. Change, 5, 475-480, doi:10.1038/nclimate2554, 2015.

Reintges, A., Martin, T., Latif, M., and Keenlyside, N. S.: Uncertainty in twenty-first century projections of the Atlantic Meridional Overturning Circulation in CMIP3 and CMIP5 models, Clim. Dyn., 49, 1495-1511, doi:10.1007/s00382-016-3180-x, 2017.

Roberts, C. D., Jackson, L., and McNeall, D.: Is the 2004-2012 reduction of the Atlantic meridional overturning circulation significant?, Geophys. Res. Lett., 41, 3204-3210, doi:10.1002/2014GL059473, 2014.

Rossby, T., Flagg, C. N., Donohue, K., Sanchez-Franks, A., and Lillibridge, J.: On the long-term stability of Gulf Stream transport based on 20 years of direct measurements, Geophys. Res. Lett., 41, 114-120, doi:10.1002/2013GL058636, 2014.

Sallenger, A. H., Doran, K. S., and Howd, P.: Hotspot of accelerated sea-level rise on the Atlantic coast of North America, Nature Clim. Change, 2, 884-888, doi:10.1038/NCILMATE1597, 2012.

Sevellec, F. and Federov, A. V.: The leading, interdecadal eigenmode of the Atlantic Meridional Overturning Circulation in a realistic ocean model, J. Clim., 26, 2160-2183, doi:10.1175/JCLI-D-11-00023.1, 2013.

Smeed, D. A., McCarthy, G., Cunningham, S. A., Frajka-Williams, E., Rayner, D., Johns, W. E., Meinen, C. S., Baringer, M. O., Moat, B. I., Duchez, A., and Bryden H. L.: Observed decline of the Atlantic Meridional Overturning Circulation 2004 to 2012, Ocean Sci., 10 (1), 29-38, doi:10.5194/os-10-29-201410, 2014.

Smeed, D. A., Josey, S. A., Beaulieu, C., Johns, W. E., Moat, B. I., Frajka-Williams, E., Rayner, D., Meinen, C. S., Baringer, M. O., Bryden, H. L., and McCarthy, G. D.: The North Atlantic Ocean is in a State of reduced overturning, Geophys. Res. Lett., 45(3), doi:10.1002/2017GL076350, 2018.

Srokosz, M., Baringer, M., Bryden, H., Cunningham, S., Delworth, T., Lozier, S., Marotzke, J., and Sutton, R., Past, present, and future changes in the Atlantic meridional overturning circulation, Bull. Amer. Met. Soc., 93, 1663-1676, doi:10.1175/BAMS-D-11-00151.1, 2012.

Taylor, A. H., and Stephens, J. A.: (1998) The North Atlantic Oscillation and the latitude of the Gulf Stream, Tellus A, 50(1), 134-142, doi:10.3402/tellusa.v50i1.14517, 1998.

Thiebaux, H. J., and Zwiers, F. W.: The interpretation and estimation of effective sample size, J. of Clim. and Appl. Met., 23, 800-811, 1984.

Valle-Levinson, A., Dutton, A., and Martin, J. B.: Spatial and temporal variability of sea level rise hot spots over the eastern United States, Geophys. Res. Lett., 44, 7876-7882, doi:10.1002/2017GL0739262017, 2017.

Woodworth, P. L., and Player, R.: The permanent service for mean sea level: an update to the 21st century, J. Coastal Res., 19(2), 287–295, 2003.

Woodworth, P. L., Maqueda, M. M., Gehrels, W. R., Roussenov, V. M., Williams, R. G., and Hughes, C. W.: Variations in the difference between mean sea level measured either side of Cape Hatteras and their relation to the North Atlantic Oscillation, Clim. Dyn., 49(7-8), 2451-2469, doi:10.1007/s00382-016-3464-1, 2016.

Woodworth, P. L., Menéndez, M., and Gehrels, W. R.: Evidence for century-timescale acceleration in mean sea levels and for recent changes in extreme sea levels, Surv. Geophys., 32, 603-618, doi:10.1007/s10712-011-9112-8, 2011.

Wu, Z., Huang, N. E., Long, S. R., Peng, C.-K.: On the trend, detrending and variability of nonlinear and non-stationary time series, Proc. Nat. Acad. Sci., 104, 14889-14894, doi:10.1073/pnas.0701020104, 2007.

Wu, Z., and Huang, N. E.: Ensemble empirical mode decomposition: a noise-assisted data analysis method, Adv. Adapt. Data Analys., 1(01), 1-41, 2009.

Yin, J., and Goddard, P. B.: Oceanic control of sea level rise patterns along the East Coast of the United States, Geophys. Res. Lett., 40, 5514-5520, doi:10.1002/2013GL057992, 2013.

Zhang, W., Chai, F., Xue, H., Oey, L.-Y.: Remote sensing linear trends of the Gulf Stream from 1993 to 2016, Ocean Dyn., doi:10.1007/s10236-020-01356-6, 2020.

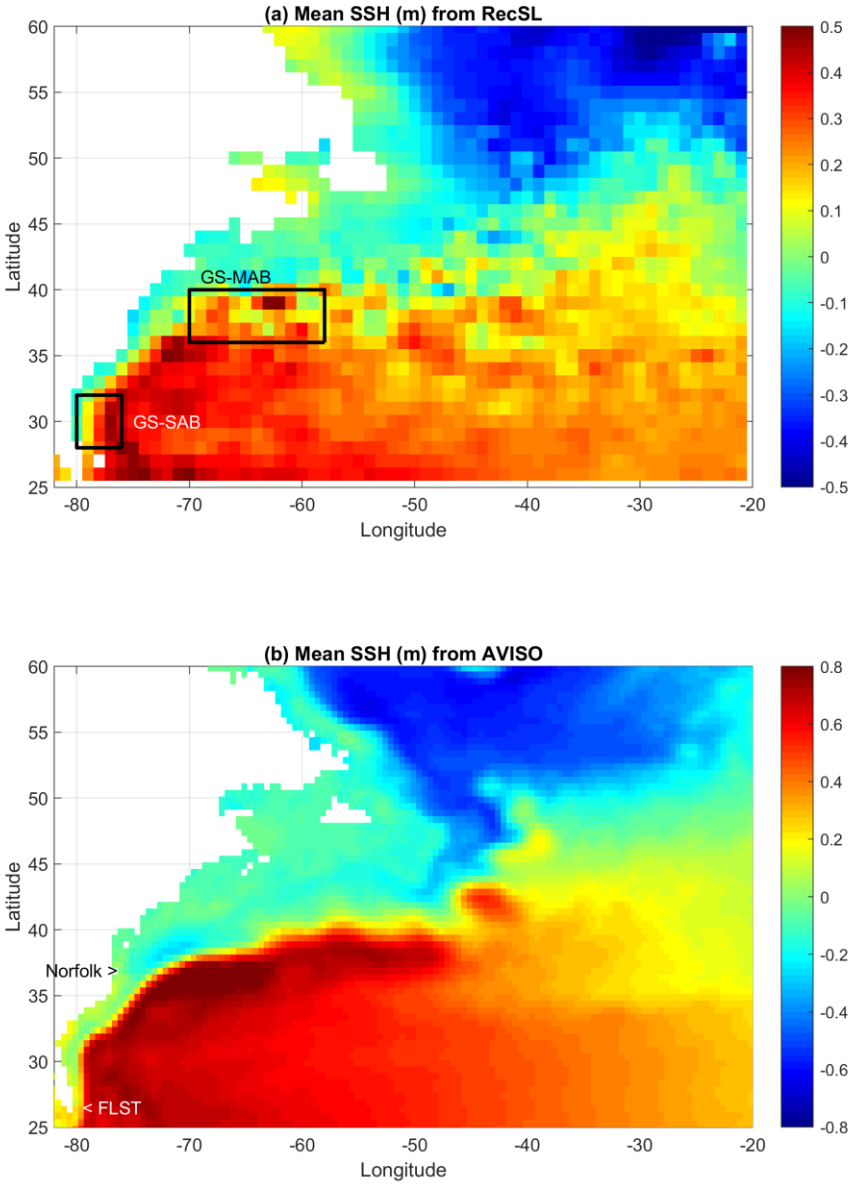

Fig. 1. Mean sea surface height in the North Atlantic Ocean during the satellite era (1993-2015) obtained from (a) the RecSL reconstruction on a 1°×1° grid and (b) the AVISO altimeter data on a 1/4°×1/4° grid. Note the different color scale. The regions where the proxy Gulf Stream is defined in the Mid-Atlantic Bight (MAB) and the South Atlantic Bight (SAB) are marked in (a) and the location of the observations of the Norfolk sea level and the Florida Current transport at the Florida Straits (FLST) are marked in (b).

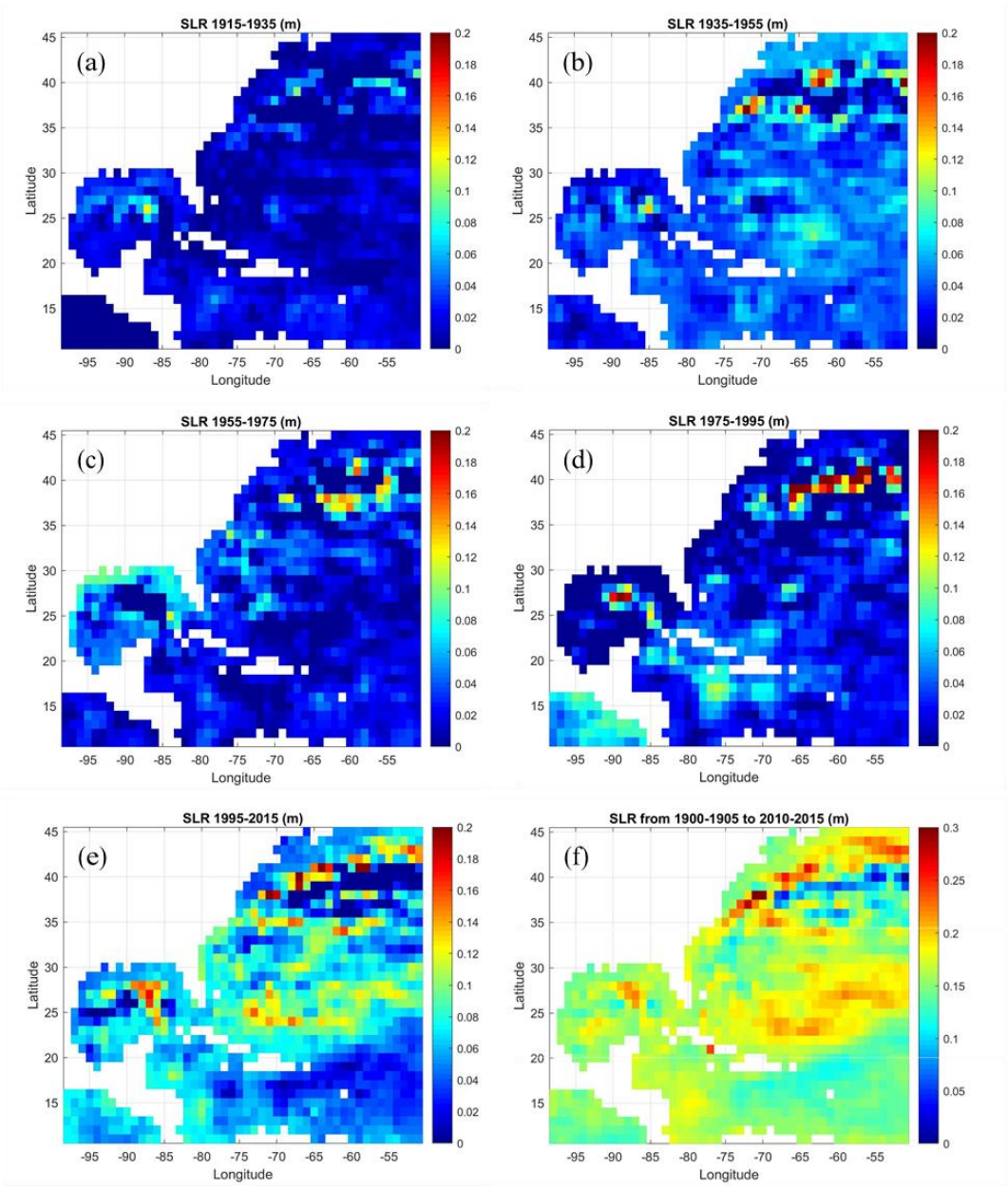

739

740 Fig. 2. (a)-(e) Sea level change at different periods. (a) The difference between the mean sea level in
741 1915 and the mean sea level in 1935, (b) for 1935-1955, (c) for 1955-1975, (d) for 1975-1995, (e) for
742 1995-2015. Note that the maximum sea level change in the colorbar, 0.2m/20 years, is equivalent to a
743 sea level rise of 10 mm/y. (f) Sea level change between the first and last 5 years of the record (note the
744 different color scale).

745

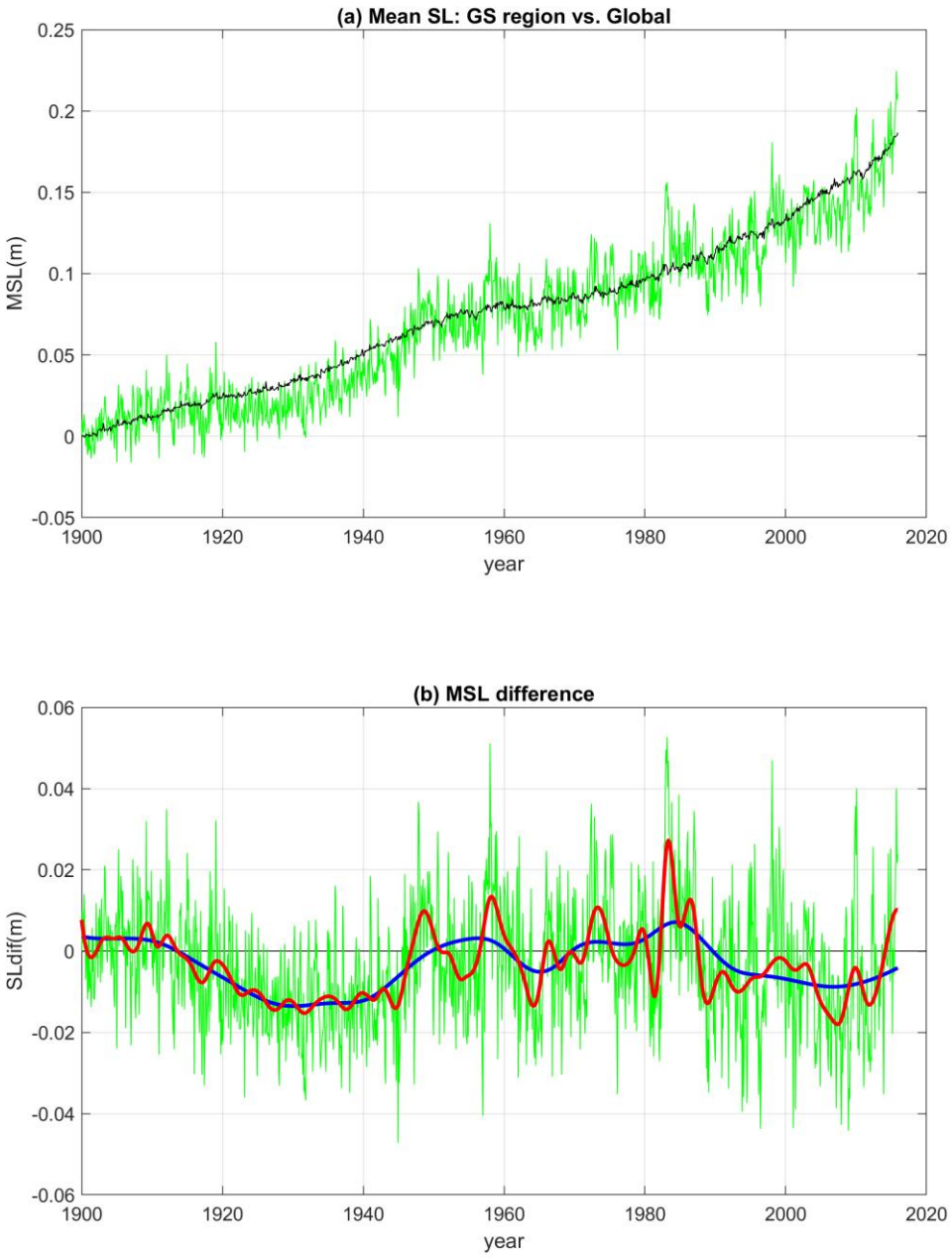

Fig. 3. (a) Global mean sea level (black line) and regional mean sea level over the area shown in Fig. 2 (green line). (b) Difference between the monthly regional and global mean sea levels (green line). Heavy red and blue lines represent low pass filtered records obtained from the sum of EMD modes with time scales longer than ~5 years and ~10 years, respectively.

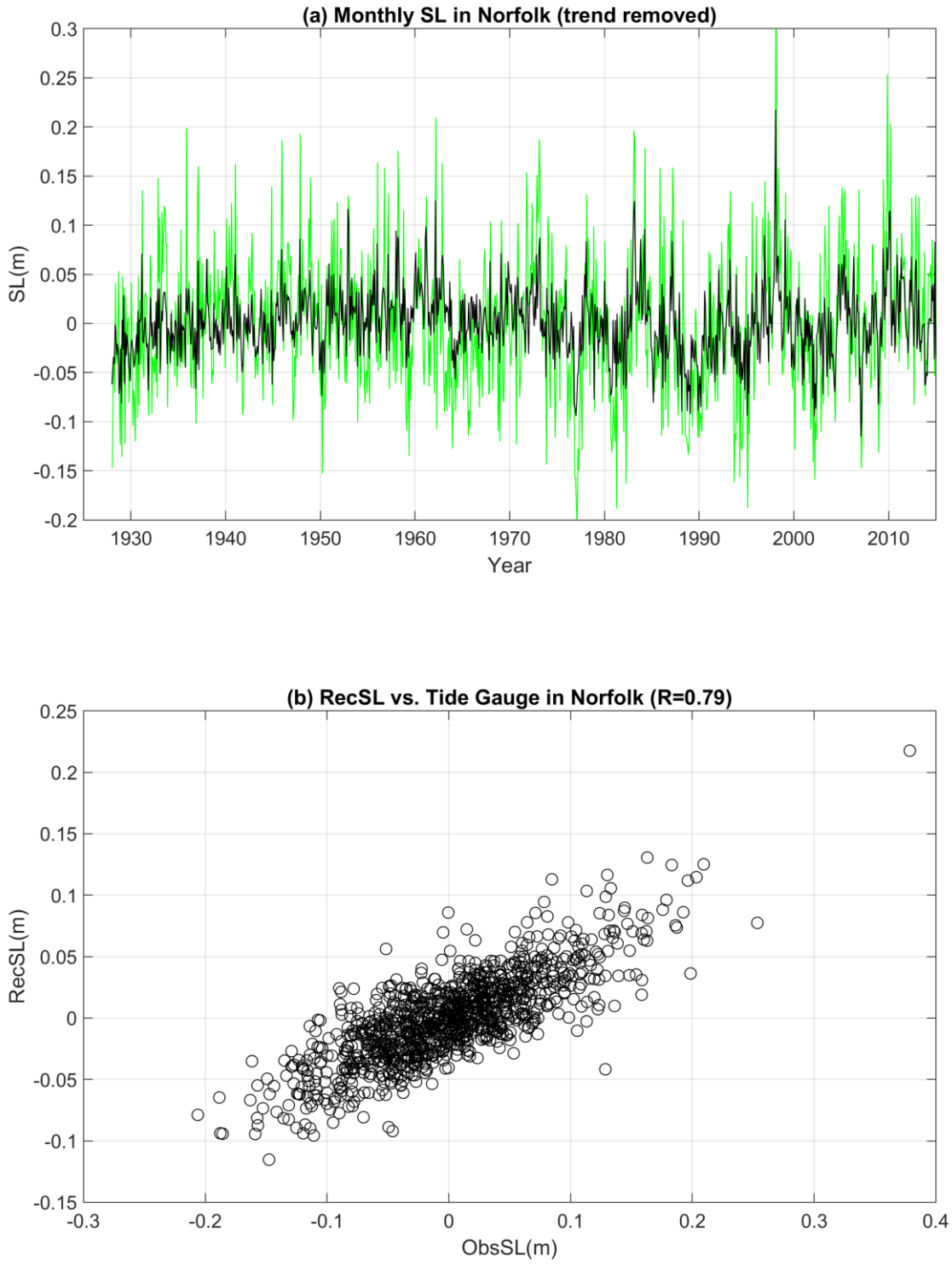

Fig. 4. (a) Comparison of the monthly observed coastal sea level (green line) at the tide gauge near Norfolk, VA (76.33°W, 36.95°N; see Fig. 1) and the reconstructed sea level (black line) in the closest 1°×1° box near the coast. (b) Scatter plot of the data comparison. The trend and the seasonal cycle were removed from both time series.

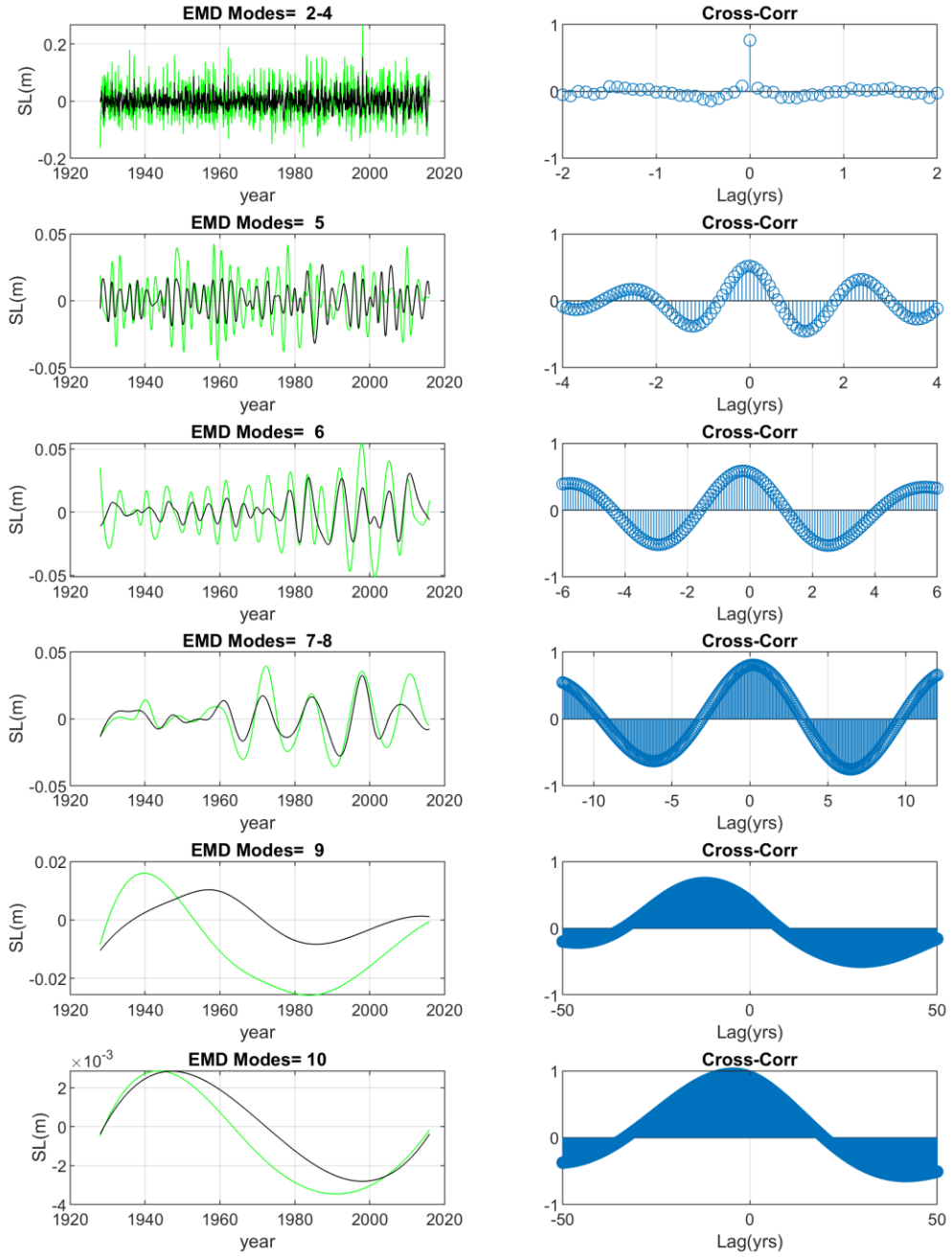

Fig. 5. Left panels: EMD oscillating modes of the observed Norfolk sea level (green) and the reconstructed sea level (black). Right panels: Cross-correlation as a function of lag. High to low frequency modes are from top to bottom panels.

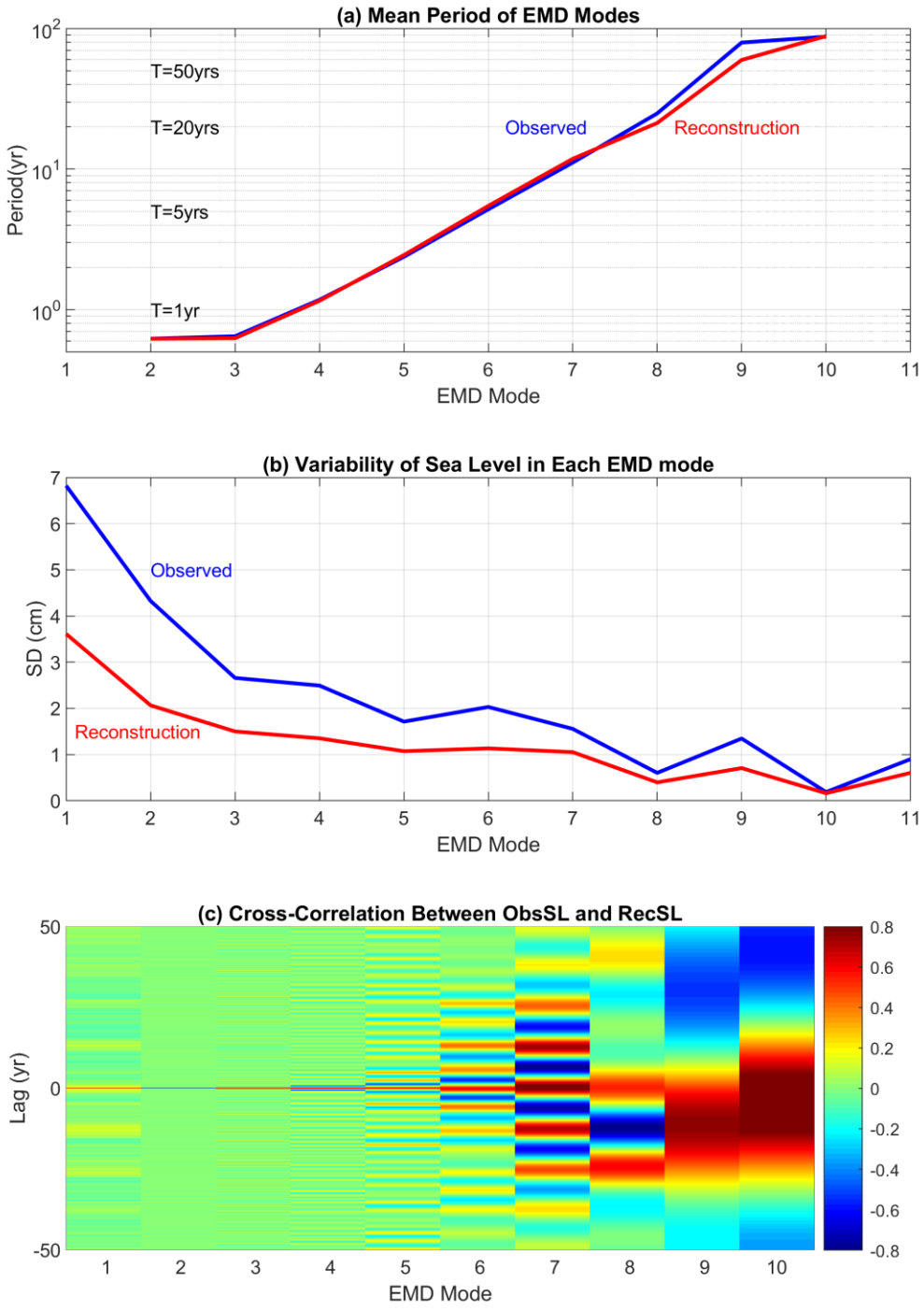

Fig. 6. (a) Mean period of the EMD oscillating modes for the observed sea level (blue) and the reconstructed sea level (red). (b) Standard deviation of each EMD mode. (c) The cross-correlation between the observed and reconstructed sea level as function of EMD modes and lag. Note that mode 1 is the original time series, modes 2-10 are oscillating modes (with time-dependent amplitude and frequency) and mode 11 is the trend.

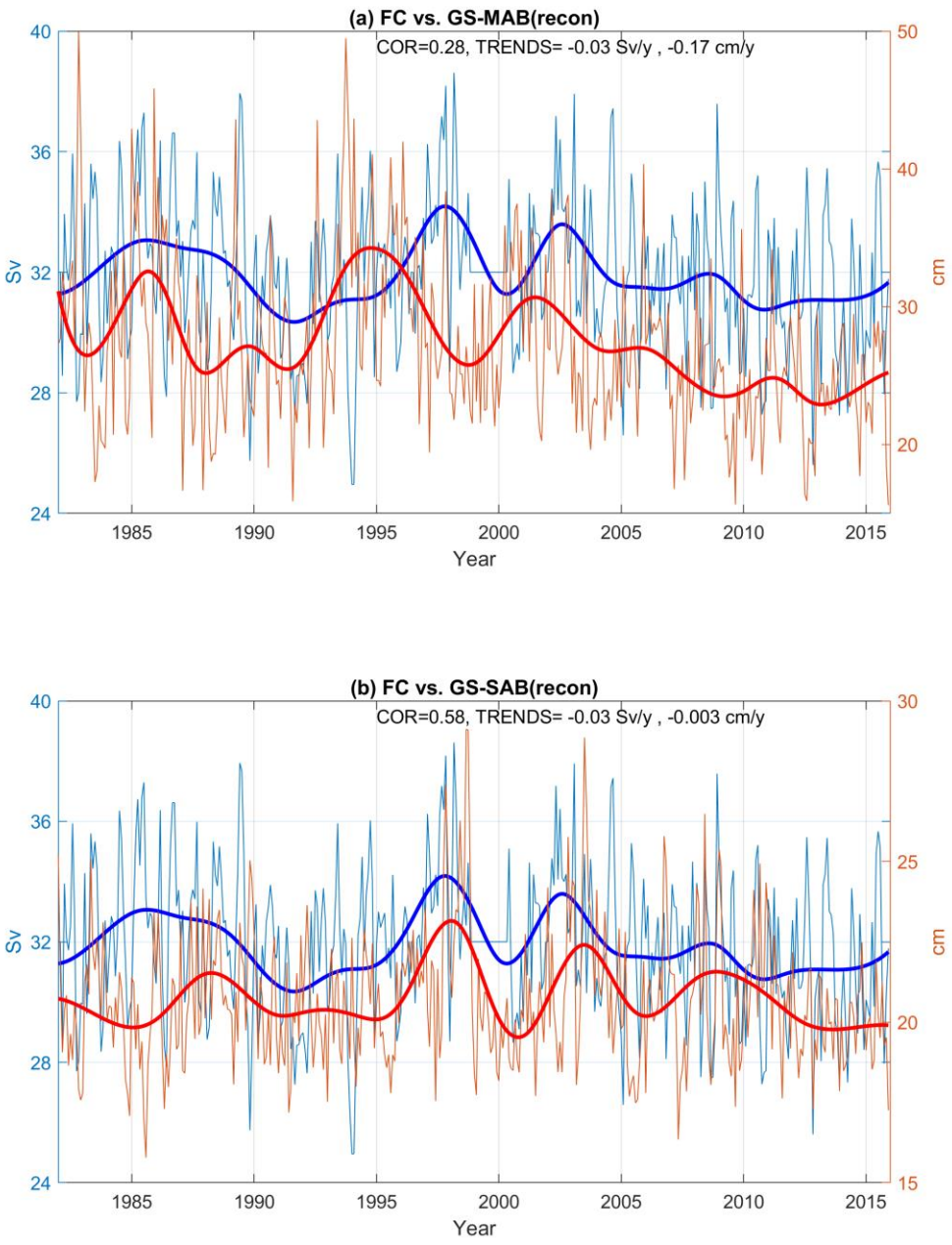

769

770 Fig. 7. Comparisons between the observed monthly Florida Current transport (blue, in Sv units on the
771 left) and the GS proxy (red, in cm sea level change units on the right) obtained from the reconstructed
772 sea level difference across the GS for (a) eastward velocity in the GS-MAB and (b) northward velocity
773 in the GS-SAB. Thin lines are monthly values and the heavy lines are low-pass filtered records (sum of
774 low frequency EMD modes). The correlation of the low frequency modes and the trends of the monthly
775 records are indicated.

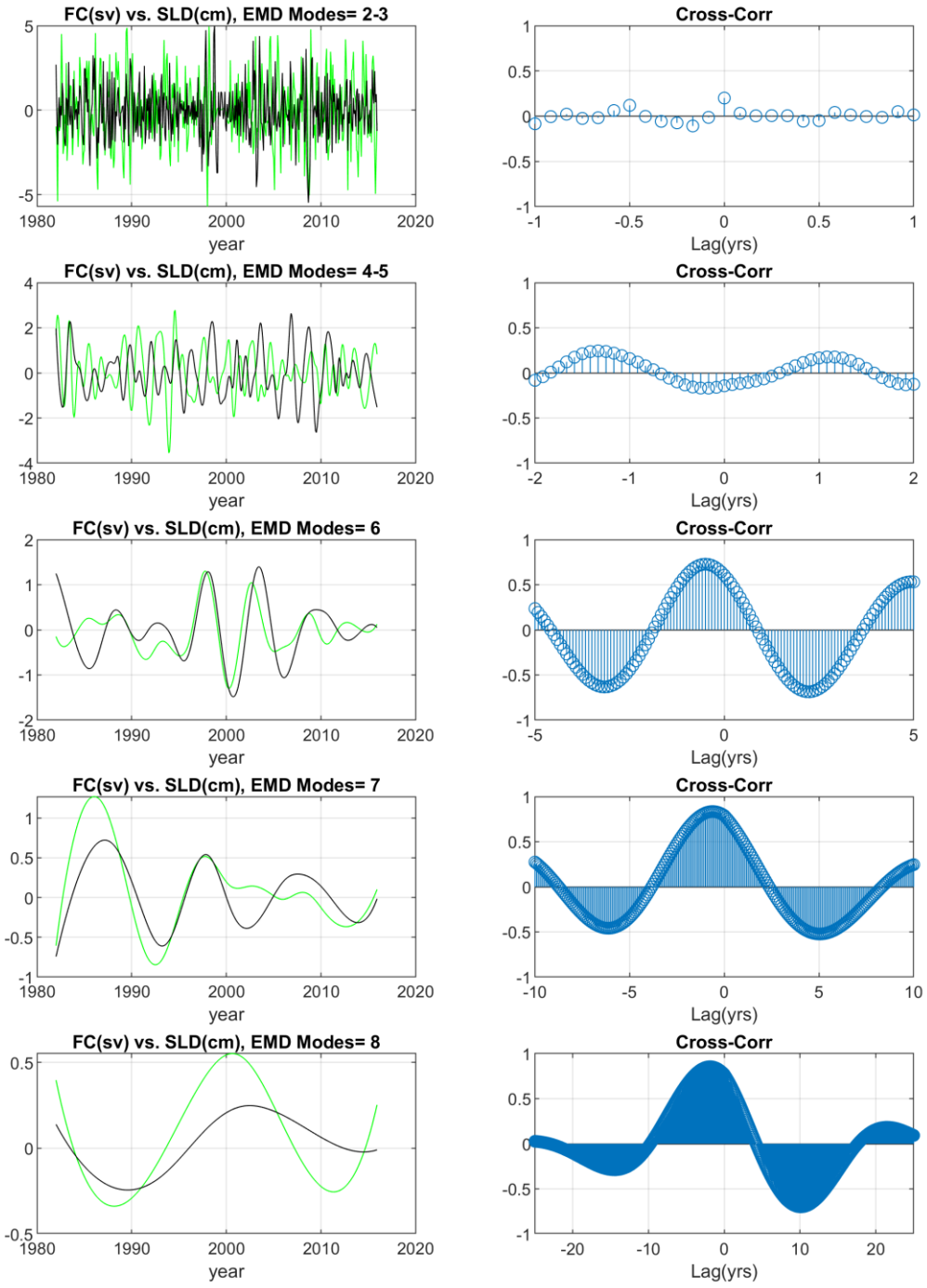

Fig. 8. Left panels: EMD oscillating modes of the observed Florida Current transport (green, in Sv) and GS-SAB proxy from the reconstructed sea level (black, in cm). Right panels: Cross-correlation as a function of lag. High to low frequency modes are from top to bottom panels.

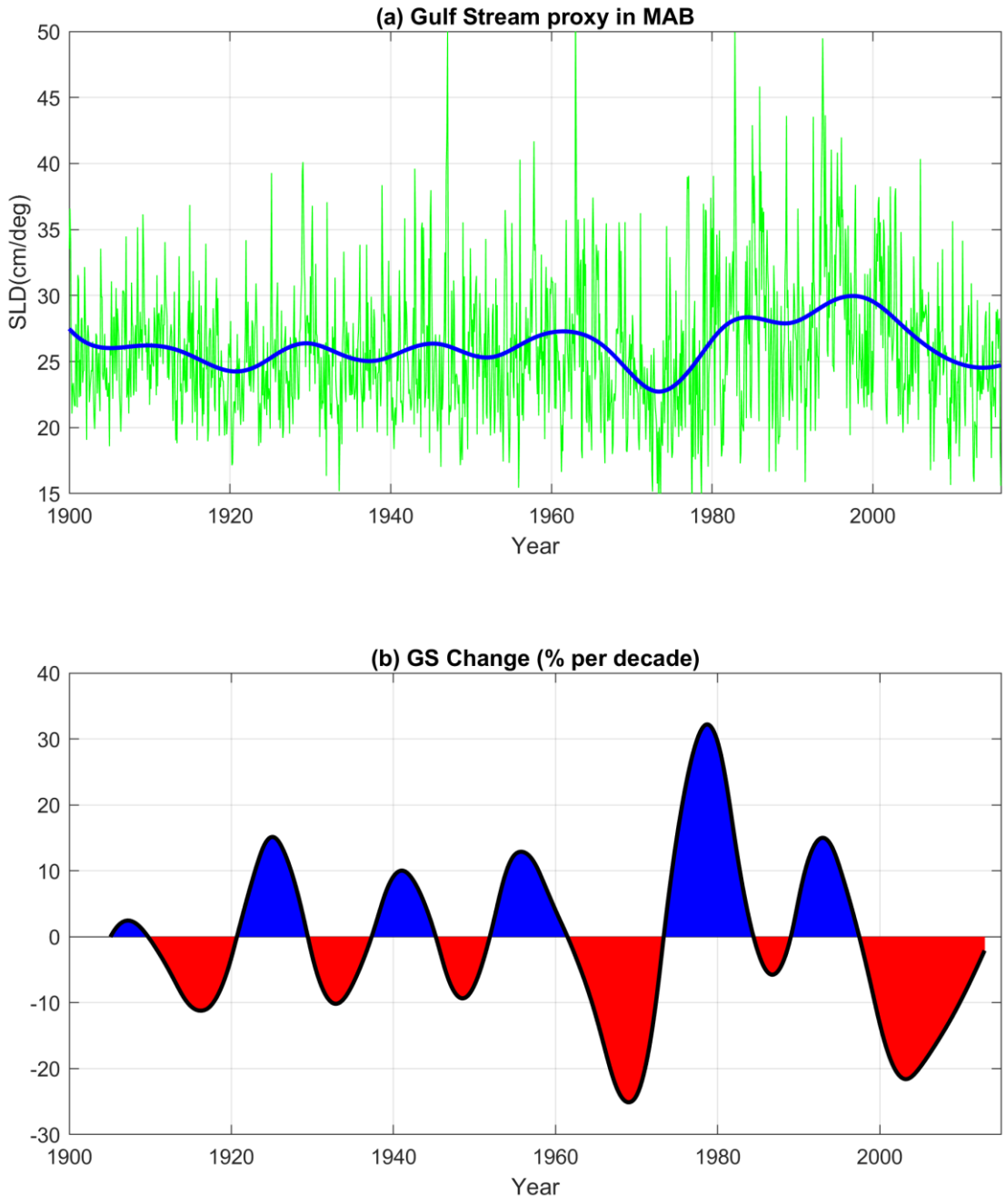

Fig. 9. (a) Gulf Stream proxy in the Mid-Atlantic Bight (GS-MAB) calculated from the average change in sea level across the GS; the units are cm change per 1° latitude. Green line is for monthly values and blue heavy line is the sum of low-frequency EMD modes. (b) The change in the strength of the GS of the low-frequency modes in (a); the units are percentage change per decade with red/blue represent periods of weakening/strengthening of the GS flow.

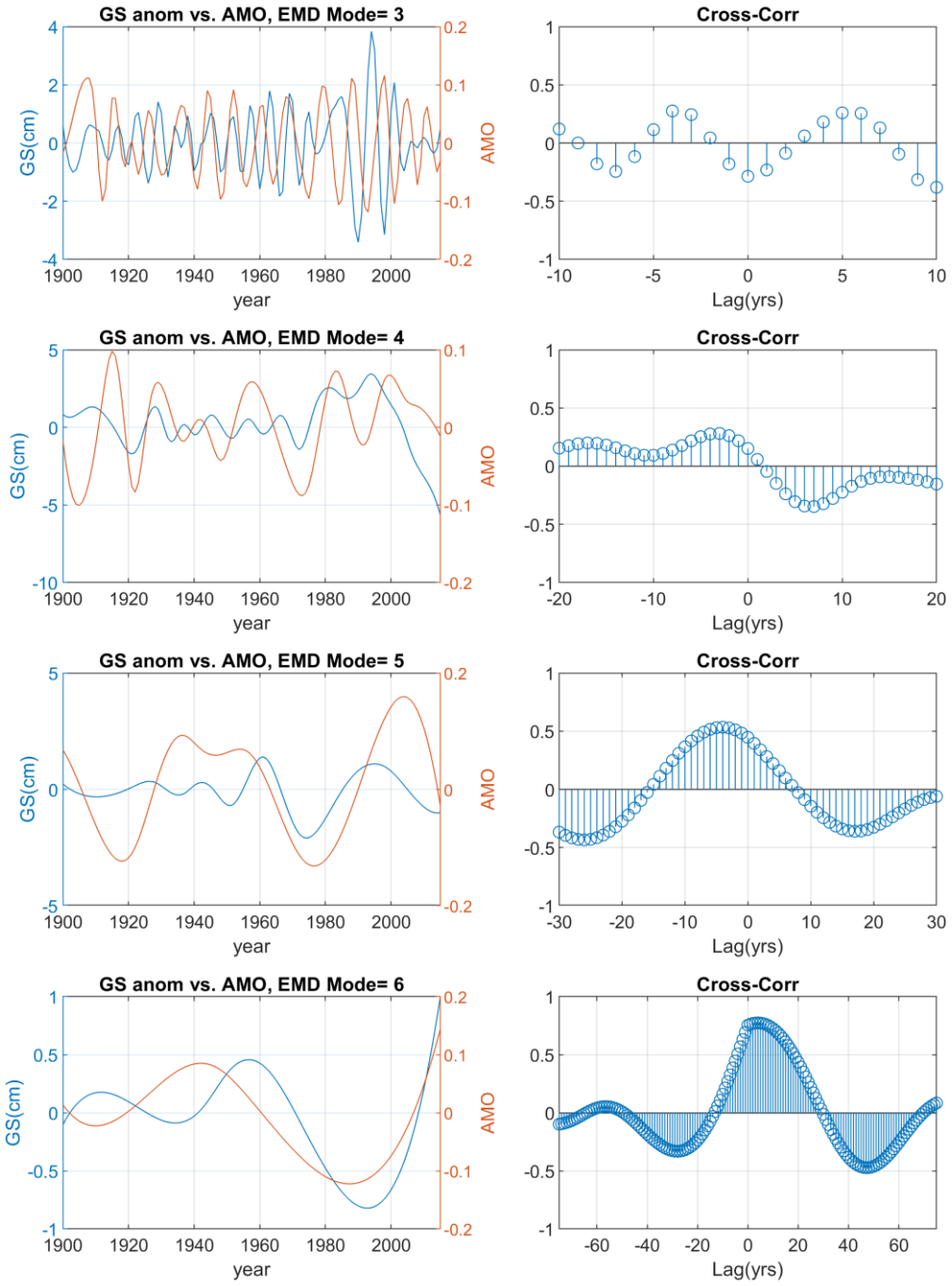

Fig. 10. (a) Comparison of EMD oscillating modes of the annual GS-MAB proxy (blue; units: sea level change across the GS in cm per degree latitude) and the annual AMO index (red). (b) Cross correlation as a function of lag. There are total 7 EMD modes; modes 2-6 are the oscillating modes.

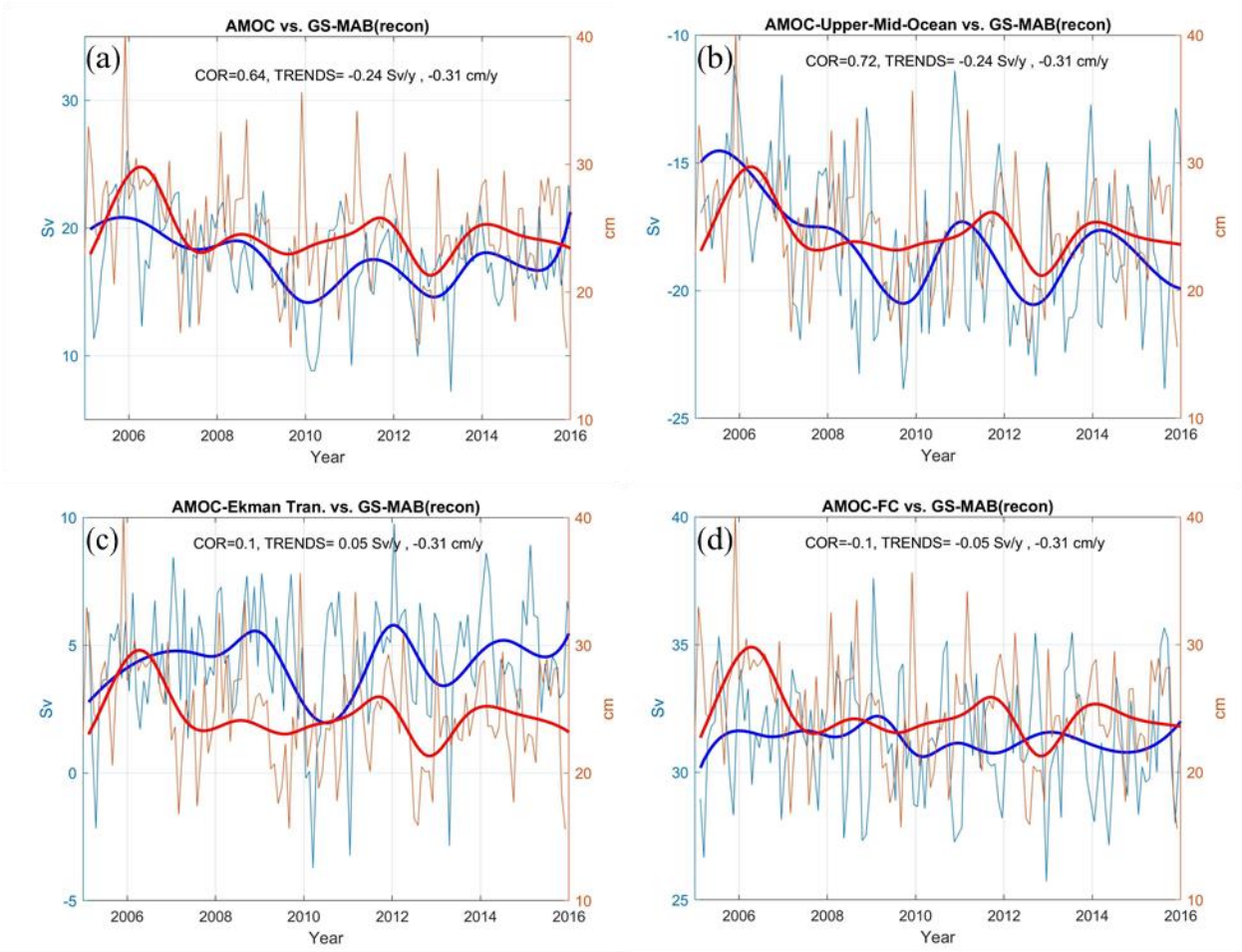

Fig. 11. Comparison between the GS-MAB proxy and the RAPID observations: (a) total AMOC transport, (b) upper mid-ocean transport, (c) Ekman transport and (d) the Florida Current transport. The GS proxy (in blue) is the average north-south sea level change across the GS (in cm per 1° latitude) representing the eastward flowing strength of the geostrophic surface flow; RAPID observations (transport in Sv) are in red. Thin lines are monthly values and the heavy lines are sum of low frequency EMD modes. The correlation of the low frequency modes and the trends of the monthly records are indicated.

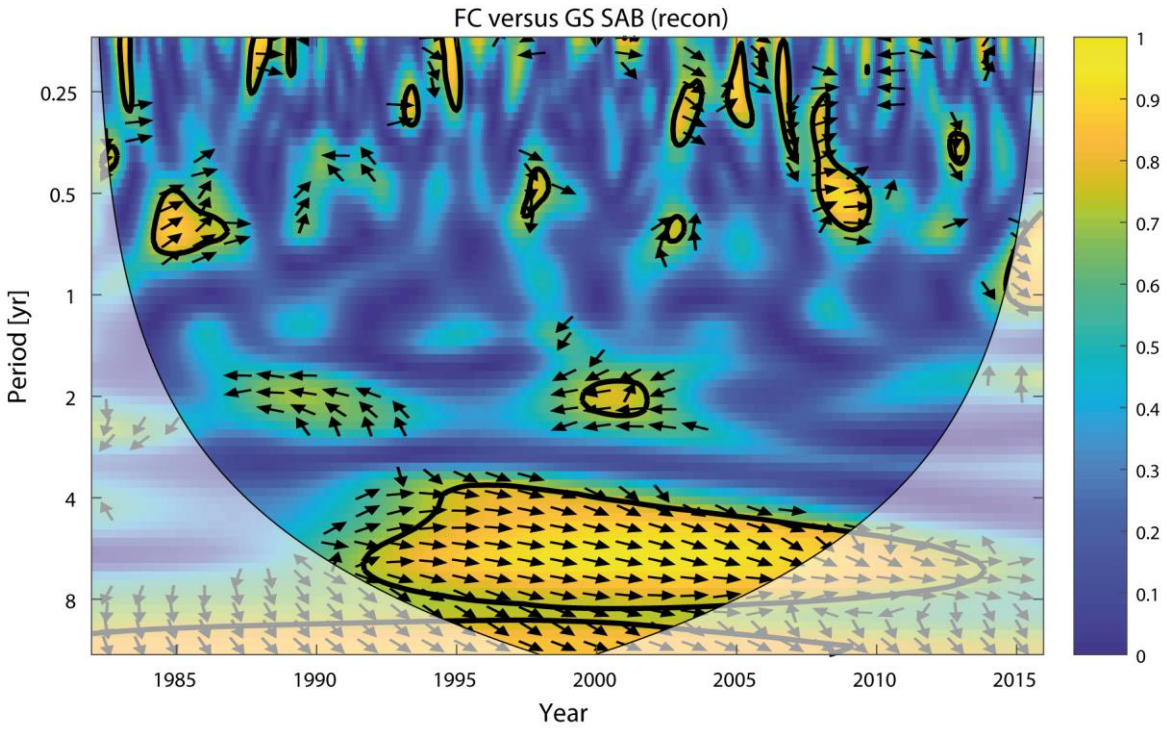

Fig. S1. Squared wavelet coherence between the standardized FC and GS-SAB time series. The 5% significance level against red noise is shown as a thick contour. All significant sections above 4 years show in-phase behavior, which is indicated by arrows that are directed to the right.

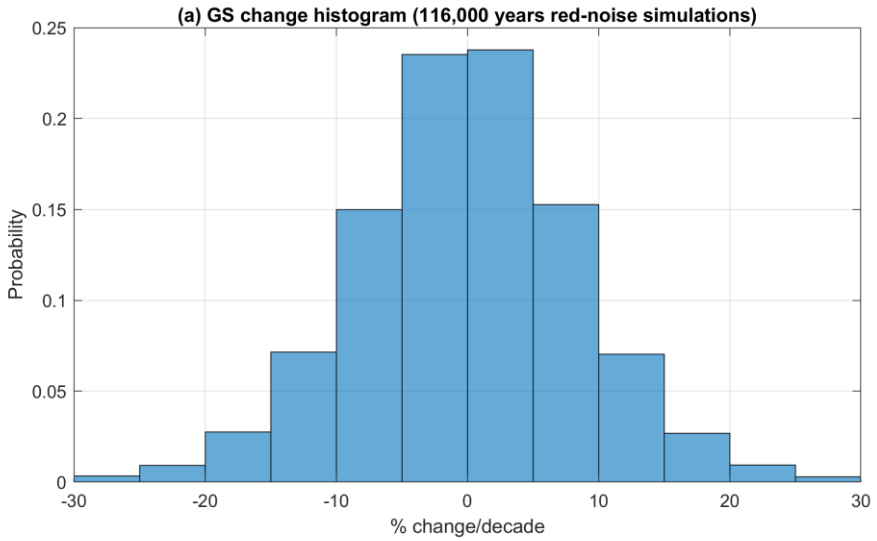

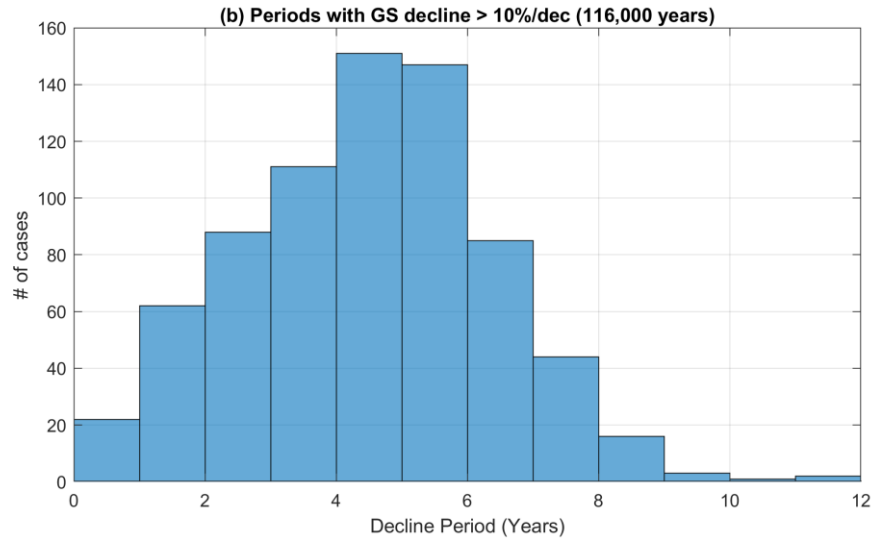

Fig. S2. Histogram of the statistics of the GS-MAB flow changes using 1000 realizations of 116 years with random red noise (total of 116,000 years); the simulations imitate the spectrum of the reconstructed GS in Fig. 9a. In each of these simulations GS change was calculated using EMD as in Fig. 9b. (a) The probability of obtaining different GS changes shows that the chance of GS weakening by over 20%/decade (as seen in the reconstruction) is less than 1% for any particular month. (b) The distribution of period length with GS flow declining by at least 10%/decade shows that there were only 3 cases of GS weakening that last at least 10 years during the 116,000 years. For comparison, the GS-MAB in Fig. 9b shows 2 such cases in 116 years, ~10 year weakening period in the 1970s and ~15 year weakening period in the 2000s.

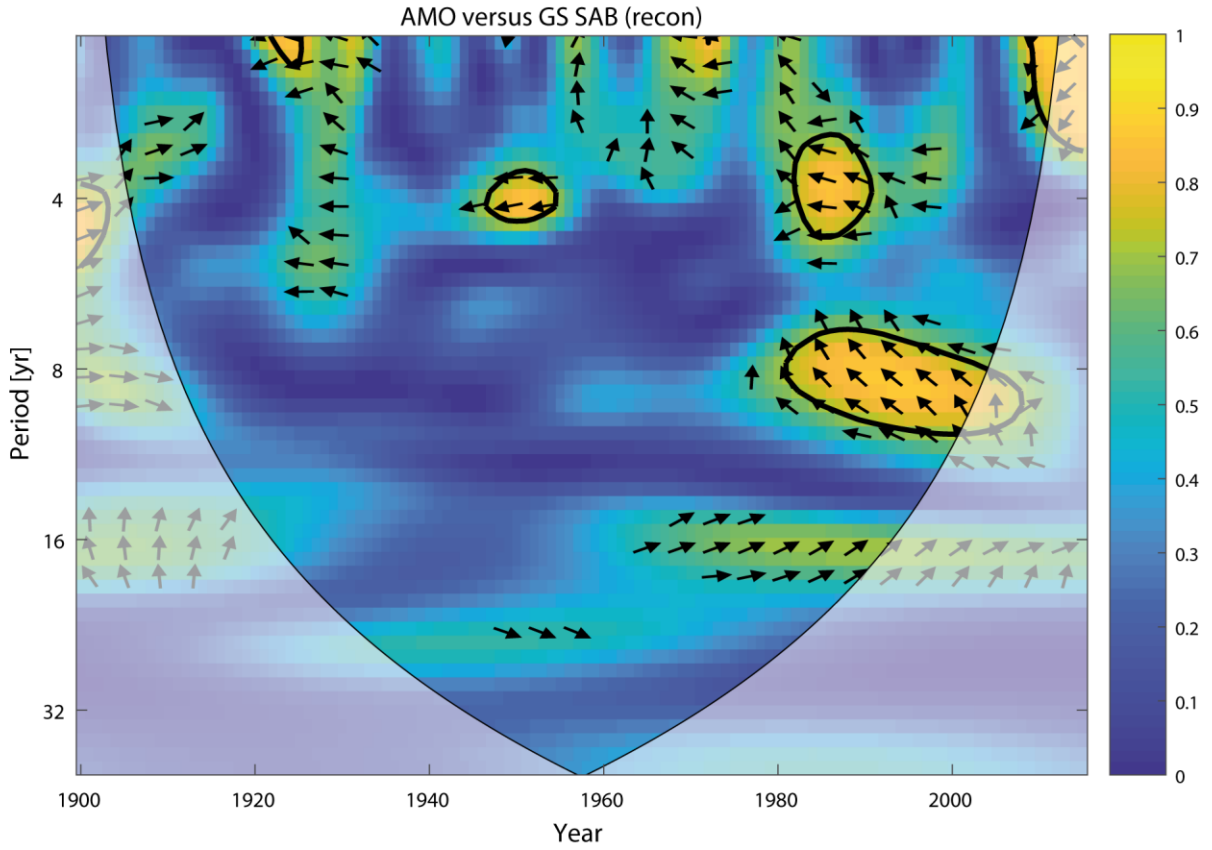

Fig. S3. Squared wavelet coherence between the standardized AMO and GS-MAB time series. The 5% significance level against red noise is shown as a thick contour. All significant sections below 10 years show anti-phase behavior, which is indicated by arrows that are directed to the left. Positive, through statistically non-significant, correlations are found in the 16-year bands since the 1960s and confirm the low-frequency modes identified by the EMD in the main paper.